
Statistische Analyse der atmosphärischen Turbulenz und allgemeiner stochastischer Prozesse

Frank Böttcher

Von Fakultät für Mathematik und Naturwissenschaften
der Carl von Ossietzky Universität Oldenburg
zur Erlangung des Grades und Titels eines

DOKTOR DER NATURWISSENSCHAFTEN
DR. RER. NAT.

angenommene Dissertation

von Herrn Frank Böttcher
geboren am 17.02.1975 in Nienburg/Weser

Gutachter: Prof. Dr. Joachim Peinke

Zweitgutachter: Priv. Doz. Dr. Achim Kittel

Tag der Disputation: 22.02.2005

Inhaltsverzeichnis

Zusammenfassung – Abstract	vi
1 Einleitung	1
1.1 Theorie der Turbulenz	1
1.2 Turbulenz in der Atmosphäre	5
Literaturverzeichnis	11
2 Analysis of Velocity Increments in the Atmosphere	13
2.1 Introduction	13
2.2 Probabilistic Description of Wind Gusts	15
2.3 Waiting Time Distribution	20
2.4 Discussion and Summary	21
Bibliography	23
3 Superposition Modell for Atmospheric Wind Speeds	25
3.1 Introduction	25
3.2 The Data	27
3.3 Analysis	29
3.3.1 Scaling in Isotropic and Atmospheric Turbulence	29
3.3.2 Probability Density Functions in Turbulence	31
3.3.3 Stable Distributions	34
3.4 Superposition Model for Atmospheric Turbulence	36
3.5 Conclusions	41
Bibliography	42
4 Determination of Measurement Noise	45
4.1 Introduction	45
4.2 The Langevin Equation	46
4.3 Measurement Noise	49
4.4 Offset of the Conditional Moments	51
4.5 Summary	55
Bibliography	56

A	Gust Definitions	59
B	Superstatistics	61
C	Offset of the Conditional Moments	63
	Danksagung	65

Abbildungsverzeichnis

1.1	Strukturfunktion 2. Ordnung	7
1.2	Zeitlicher Verlauf einer Windböe nach IEC Norm	8
2.1	Typical Wind Speed Time Series	16
2.2	Increment PDFs of Atmospheric Data	17
2.3	Comparison between Gaussian and Intermittent Distributions	18
2.4	PDFs of the Laboratory and Conditioned Atmospheric Data	19
2.5	λ^2 as a Function of Scale for Laboratory and Atmospheric Data	20
2.6	Waiting Time Distributions of Wind Gusts	21
3.1	Scaling Exponents and Structure Functions	30
3.2	Flatness as a Function of Scale	31
3.3	Comparison between PDFs of Laboratory and Atmospheric Increments	32
3.4	λ^2 for different Data Sets	34
3.5	Illustration of the Superposition of different Mean Wind Speeds	36
3.6	Distribution of the Mean Wind Speed for different Atmospheric Data Sets	37
3.7	Standard Deviation σ_0 as a Function of \bar{u}	38
3.8	Reconstruction of Atmospheric and Laboratory Increment PDFs	40
4.1	Increment PDF of a Multiplicative Cascade Process	48
4.2	Influence of Measurement Noise on $M^{(1)}$	50
4.3	Illustration of a Langevin Process with Superimposed Measurement Noise	52
4.4	Offset of the First Conditional Moment $M^{(1)}$	53
4.5	Offset of the Second Conditional Moment $M^{(2)}$	54

Zusammenfassung

Diese Arbeit beschäftigt sich im Wesentlichen mit der Charakterisierung atmosphärischer Turbulenz. Als ein herausragendes Problem wird die stark anomale, intermittente Statistik der Geschwindigkeitsdifferenzen – der so genannten Geschwindigkeitsinkremente – untersucht und ihre Relevanz für die Abschätzung von Extremereignissen diskutiert.

Es wird gezeigt, dass sich die Statistik atmosphärischer Geschwindigkeitsinkremente derjenigen stationärer, homogener und isotroper Turbulenz annähert, wenn die auf eine mittlere Geschwindigkeit bedingten Inkremente betrachtet werden. Darüber hinaus wird ein neues Modell vorgestellt, das die Inkrementstatistik in der Atmosphäre als Überlagerung verschiedener homogener und isotroper Abschnitte beschreibt. Die Verteilung dieser Abschnitte wird durch eine Weibullverteilung beschrieben, die allgemein als jährliche Verteilung der mittleren Windgeschwindigkeiten angenommen wird.

Als ein weiterer Aspekt wird das grundlegende Problem von Messrauschen bei der Analyse von experimentellen Zeitserien diskutiert. Es zeigt sich, dass Messrauschen vom intrinsischen, dynamischen Rauschen unterschieden werden kann und sich der gesamte Übergangsbereich von rein dynamischem Rauschen bis hin zu reinem Messrauschen charakterisieren lässt.

Abstract

The essential part of this work is devoted to a proper characterization of atmospheric turbulence. Being an outstanding problem, the markedly intermittent statistics of velocity differences – the velocity increments – will be examined and their relevance in view of estimating extreme events will be discussed.

Considering the statistics of increments that are conditioned on a certain averaged wind speed the statistics approach those of stationary, homogeneous and isotropic turbulence. In addition to that a new model will be presented in which the atmospheric increment statistics are explained as a superposition of different subsets of homogeneous and isotropic turbulence. It will be shown that these subsets are distributed according to a Weibull distribution which is commonly considered to be the annual distribution of averaged wind speeds.

A second emphasis is placed on the fundamental problem of the influence of measurement noise in experimental time series. It will be shown that by analyzing experimental time series measurement noise can be distinguished well from the intrinsic dynamical noise. It is found that the whole transition range from pure dynamical to pure measurement noise can be characterized.

Kapitel 1

Einleitung

1.1 Theorie der Turbulenz

Turbulente Strömungen sind ein alltägliches Phänomen. Sie zeichnen sich durch regellos erscheinende Wirbelstrukturen aus, die im Gegensatz zu laminaren Strömungen chaotisch und unvorhersehbar erscheinen. Dennoch lassen sich bei genauerer Betrachtung wiederkehrende Strukturen auf unterschiedlichsten Größenskalen erkennen, eine Eigenschaft, die oftmals mit dem Begriff *Selbstähnlichkeit* oder *Fraktalität* beschrieben wird. Turbulente Strömungen lassen sich in einer Vielzahl unterschiedlichster Systeme wiederfinden, sei es in fließenden Gewässern, in der Rauchfahne eines Schornsteins oder in den Sonnenwinden unseres Zentralgestirns. Zudem spielen sie eine entscheidende Rolle bei der Durchmischung von Gasen und bestimmen wesentlich die Transporteigenschaften innerhalb einer Strömung.

Aufgrund der Allgegenwärtigkeit des Phänomens besteht ein großes Interesse an einer quantitativen Beschreibung turbulenter Strömungen. Diese lassen sich prinzipiell mit der seit etwa 150 Jahren bekannten *Navier-Stokes-Gleichung* beschreiben, die die allgemeine Bewegungsgleichung für Fluide darstellt. Allerdings sind nur wenige Spezialfälle bekannt, in denen sich die Gleichung analytisch lösen lässt.

Die Navier-Stokes-Gleichung für inkompressible Flüssigkeiten, komplettiert durch die *Kontinuitätsgleichung*, lautet:

$$\begin{aligned}\frac{\partial \mathbf{u}}{\partial t} + (\mathbf{u} \nabla) \mathbf{u} &= -\frac{1}{\rho} \nabla p + \nu \Delta \mathbf{u} \\ \nabla \cdot \mathbf{u} &= 0 \quad .\end{aligned}\tag{1.1}$$

Mit $\mathbf{u} = \mathbf{u}(\mathbf{x}, t)$ ist die vektorielle Geschwindigkeit beschrieben, ρ bezeichnet die (für inkompressible Fluide konstante) Dichte, ν die *kinematische Viskosität* und $p = p(\mathbf{x}, t)$ das skalare Druckfeld. Zudem können weitere externe Kräfte, wie beispielsweise Gravitationskräfte, auftreten, die sich in zusätzlichen Termen auf der rechten Seite der Navier-Stokes-Gleichung äußern würden.

Turbulentes Verhalten wird neben der Nichtlokalität des Druckterms durch den *Advektionsterm* $(\mathbf{u}\nabla)\mathbf{u}$ hervorgerufen, der die einzelnen Geschwindigkeitskomponenten und deren Ableitungen nichtlinear miteinander koppelt. Demgegenüber wirkt eine hohe kinematische Viskosität ν , die die Zähigkeit des Fluids beschreibt, dem Auftreten von Turbulenz entgegen und übt einen laminarisierenden Einfluss auf das Geschwindigkeitsfeld aus.

Zur Unterscheidung zwischen turbulenter und laminarer Strömung betrachtet man gemeinhin die *Reynoldszahl*:

$$Re = \frac{UL}{\nu} \quad . \quad (1.2)$$

Die Größen U und L bezeichnen eine strömungsspezifische, charakteristische Geschwindigkeit bzw. Länge. Im Falle einer Zylindernachlaufströmung beispielsweise sind dies die Anströmgeschwindigkeit und der Durchmesser des Zylinders. Die dimensionslose Reynoldszahl ist die einzig verbleibende Kenngröße, wenn man Gl. (1.1) über die Transformation

$$t_0 = t \frac{U}{L}, \quad p_0 = \frac{p}{\rho U^2}, \quad \mathbf{x}_0 = \frac{\mathbf{x}}{L}, \quad \mathbf{u}_0 = \frac{\mathbf{u}}{U} \quad (1.3)$$

in eine dimensionslose Form überführt:

$$\frac{\partial \mathbf{u}_0}{\partial t_0} + (\mathbf{u}_0 \nabla) \mathbf{u}_0 = -\nabla p_0 + \frac{1}{Re} \Delta \mathbf{u}_0 \quad . \quad (1.4)$$

Turbulente Strömungen sind im Gegensatz zu laminaren durch hohe Reynoldszahlen gekennzeichnet. Dabei hängt es stark von der betrachteten Strömung ab, bei welchen Reynoldszahlen der Umschlag in turbulentes Verhalten erfolgt.

Aufgrund der Tatsache, dass analytische Lösungen der Navier-Stokes-Gleichung nur für wenige und stark vereinfachte Situationen möglich sind und direkte numerische Simulationen (DNS) auf relativ kleine Reynoldszahlen beschränkt bleiben¹, nehmen statistische Modelle einen wichtigen Platz in der Turbulenzforschung ein.

Für eine statistische Beschreibung wird angenommen, dass die im Strömungsfeld vorliegende Energie auf großen Skalen L erzeugt und sukzessive auf kleiner werdende Skalen verteilt wird, bis sie schließlich in Form von Wärme auf den Skalen der Größe der *Kolmogorov-Länge* η dissipiert wird. Ausgehend von diesem Kaskadenprozess der turbulenten Energie, der auf die Vorstellung von L. F. Richardson [1] zurückgeht, entwickelte A. N. Kolmogorov 1941 ein mathematisches Modell, das als Grundlage der Erforschung der kleinskaligen Turbulenz angesehen werden kann [2].

¹Die Anzahl der Gitterpunkte und damit der Aufwand an Rechnerleistung steigt mit Re^3 an.

Aufgrund der räumlich hierarchischen Struktur, die dem Kaskadenmodell zugrunde liegt, wählt man als Beschreibungsgröße oftmals das *Geschwindigkeit-sinkrement* $u_r := \mathbf{e} \cdot (\mathbf{u}(\mathbf{x} + \mathbf{r}) - \mathbf{u}(\mathbf{x}))$, das die Geschwindigkeitsdifferenz in Abhängigkeit von der Skala \mathbf{r} beschreibt. Liegt die betrachtete Geschwindigkeitskomponente parallel zum Verbindungsvektor \mathbf{r} , so spricht man von *longitudinalen*, stehen sie senkrecht auf dem Verbindungsvektor von *transversalen* Inkrementen.

Aus Dimensionsüberlegungen sowie unter der Annahme räumlich homogener und isotroper Geschwindigkeitsfelder² und einer selbstähnlichen (fraktalen) Struktur turbulenter Strömungen leitete Kolmogorov 1941 die als *K41* bekannt gewordene Relation der Strukturfunktionen n -ter Ordnung S_r^n für den Inertialbereich³ her:

$$S_r^n = \langle (u_r)^n \rangle = C_n \epsilon^{\zeta_n} r^{\zeta_n} \quad . \quad (1.5)$$

Dabei verläuft der Skalenexponent mit $\zeta_n = n/3$ linear in n , C_n wird als universelle Konstante behandelt und die Energiedissipationsrate ϵ bezeichnet den als konstant angenommenen Energiefluss durch die Kaskade. Die Linearität des Skalenexponenten wird auch mit dem Begriff *Monofraktalität* beschrieben.

Es hat sich herausgestellt, dass das monofraktale Modell nur näherungsweise korrekt ist und ζ_n durch eine nichtlineare, *multifraktale* Funktion beschrieben werden sollte. Unter der Annahme einer fluktuierenden, log-normal verteilten Energiedissipationsrate entwickelten Kolmogorov und Obukhov 1962 [3] erstmals ein Modell mit nichtlinearem Skalenexponenten. Dieses auch als *K62* bekannte Modell weist einen konkaven Verlauf von ζ_n in Abhängigkeit von n auf: $\zeta_n = \frac{n}{3} - \frac{\mu}{18}n(n-3)$.

Neben dem *K62* Modell existieren weitere multifraktale Modelle, die sich wesentlich nur für große Werte von n unterscheiden. Strukturfunktionen hoher Ordnung werden jedoch zunehmend durch wenige Extremwerte der zu Grunde liegenden Zeitserie bestimmt und sind dementsprechend stark fehlerbehaftet. Hierdurch wird eine Verifikation der einzelnen multifraktalen Modelle auf Basis von Messdaten für Strukturfunktionen der Ordnung $n > 8$ sehr schwierig [4], wodurch sich die Koexistenz der verschiedenen Modelle erklärt.

Allen Modellen gemein ist die konkave Krümmung des Skalenexponenten sowie der Punkt $\zeta_3 = 1$, der sich direkt aus der exakten Beziehung

$$S_r^3 = -\frac{4}{5}\epsilon \cdot r \quad (1.6)$$

ergibt [5].

²Die Begriffe 'homogen' und 'isotrop' bezeichnen die Translations- bzw. Rotationsinvarianz der statistischen Eigenschaften innerhalb der betrachteten Strömung.

³Dieser umfasst den Skalenbereich $\eta \ll r \ll L$, wobei η durch die Energiedissipationsrate ϵ und die kinematische Viskosität ν gegeben ist: $\eta = \left(\frac{\nu^3}{\epsilon}\right)^{1/4}$.

Die Nichtlinearität des Skalenexponenten führt zu einer Verletzung der Selbstähnlichkeit der Statistik auf unterschiedlichen Skalen. Diese äußert sich am augenscheinlichsten durch eine, in Experimenten häufig beobachtete, Formänderung der Wahrscheinlichkeitsdichten der Inkremente. Dabei bewirkt die konkave Krümmung des Skalenexponenten ζ_n als Funktion von n , dass große Inkrementwerte für kleine Skalen anomal häufig auftreten. Dies wird ersichtlich, betrachtet man beispielsweise die Kurtosis $F := \langle u_r^4 \rangle / \langle u_r^2 \rangle^2 = S_r^4 / (S_r^2)^2$. Für das *K62* Modell folgt dann $F \propto r^{-4\mu/9}$. Auf kleinen Skalen erhält man somit hohe Kurtosiswerte, die eine anomale Statistik implizieren.

Die anomalen Verteilungen für kleine Skalen und die allgemeine Formänderung in Abhängigkeit der Skala werden unter dem Begriff *Intermittenz* der kleinskaligen Turbulenz zusammengefasst. Der Parameter μ wird deshalb auch als *Intermittenzfaktor* bezeichnet.

Die dargestellten Theorien und Modelle können in diversen Standardwerken zum Thema Turbulenz und Fluidodynamik nachgelesen werden. Einen guten Überblick geben beispielsweise die Werke [6],[7],[8], [9] und [10].

1.2 Turbulenz in der Atmosphäre

'It is a matter of common experience that the wind near the ground, and in fact in the first few hundred metres or so of altitude, is never steady, but is continuously disturbed by the random fluctuations known colloquially as gusts.' [11]

Der Schwerpunkt dieser Arbeit liegt in der Erforschung der Intermittenz kleinskaliger Turbulenz in der atmosphärischen Grenzschicht. Dabei wird Turbulenz in der atmosphärischen Grenzschichtströmung im Wesentlichen durch Scherung des Windfeldes mit der Erdoberfläche erzeugt. Desweiteren kommt es je nach orographischen Gegebenheiten und thermischer Stabilität zu zusätzlichen turbulenten Nachlauf- und Auftriebsströmungen, wodurch sich die enorme Komplexität atmosphärischer Turbulenz begründet.

Aufgrund der großen Dimensionen werden in der Atmosphäre sehr hohe Reynoldszahlen erreicht. Setzt man $100m$ bis $1000m$ als obere Grenze der größten Wirbelstrukturen an, was in etwa der Höhe der Grenzschicht entspricht sowie eine mittlere Windgeschwindigkeit von $10ms^{-1}$, so ergeben sich typische Reynoldszahlen von $Re \approx 10^8$ bis $Re \approx 10^9$. Große Reynoldszahlen rufen einen ausgeprägten Inertialbereich hervor, in dem die Statistik als unabhängig von den jeweiligen Randbedingungen der Turbulenz erzeugenden Strömung angenommen wird. Vor diesem Hintergrund sollte die Statistik stationärer, homogener und isotroper turbulenter Geschwindigkeitsfelder, die in Laborexperimenten unter wohldefinierbaren Bedingungen erzeugt werden, mit der Statistik atmosphärischer Geschwindigkeiten prinzipiell vergleichbar sein.

Das wesentliche Problem bei der Analyse atmosphärischer Geschwindigkeiten besteht in ihrer Instationarität, die durch die enorme Variabilität der großskaligen Luftströmungen hervorgerufen wird. Während sich in Laborexperimenten stationäre, homogene und isotrope Strömungen verhältnismäßig leicht realisieren lassen, ist dies in der Atmosphäre bestenfalls näherungsweise und nur für kurze Zeitabschnitte möglich. Im Allgemeinen werden sich sowohl die Windgeschwindigkeit als auch die Windrichtung permanent ändern. Damit sind beide Größen nicht eindeutig definiert und können nur als Mittelwerte angegeben werden. Auf diese Problematik hat L. F. Richardson bereits 1926 [12] mit der provokativen Frage *'Hat der Wind eine Geschwindigkeit?'* hingewiesen.

Der allgemeine Ansatz die Windgeschwindigkeit zu erfassen besteht darin, sie in einen mittleren, langsam variierenden Anteil und einen überlagerten, turbulenten Anteil zu zerlegen. Damit lässt sie sich darstellen als $u(t) = \bar{u}(t) + u'(t)$. Auf eine vektorielle Erfassung wird zumeist verzichtet, so dass mit u die Komponente in Richtung der mittleren Geschwindigkeit bezeichnet ist. Zur Bestimmung von \bar{u} wird über den Zeitraum T integriert. Problematisch ist hierbei die Festlegung eines adäquaten Zeitraumes T , der im Prinzip frei wählbar ist.

Mitte des vergangenen Jahrhunderts wurde aus atmosphärischen Geschwindigkeitsdaten erstmals ein Spektrum erstellt [13]. In diesem erkannte man eine *spektrale Lücke*, d.h. einen Bereich geringer Energiedichte für Periodizitäten zwischen $5min$ und $5h$ sowie drei lokale Maxima bei Periodizitäten von etwa $100h$, $12h$ und $1min$. Diese werden als die typische Dauer von Wetterlagen, als Halbtagszyklus und als kleinskalige atmosphärische Turbulenz interpretiert. In diesem Spektrum erscheint die spektrale Lücke demnach als natürliche Trennung zwischen groß- und kleinskaligen Ereignissen und scheint eine Rechtfertigung für Mittelungszeiten von $10min$ bis $1h$ zu liefern, die von vielen Autoren im Bereich der Meteorologie vorgeschlagen werden (z.B. [14], [15], [16]).

Der Verlauf der spektralen Lücke scheint allerdings geographischen und zeitlichen Schwankungen unterworfen zu sein (e.g. [17], [18]) und teilweise wird ihre Existenz überhaupt bestritten (z.B. [19], [20]).

Für die in dieser Arbeit untersuchten Datensätze lässt sich kein klarer Hinweis auf die Existenz einer spektralen Lücke finden. Diese sollte sich zum Beispiel in einem Bereich konstanter Werte der Strukturfunktionen widerspiegeln, der dem Skalenbereich der spektralen Lücke entspricht. Abweichend von der in der Turbulenzforschung üblichen räumlichen Betrachtung werden die Inkremente im Folgenden über der zeitlichen Skala τ betrachtet⁴. In Abb. 1.1 ist exemplarisch die Strukturfunktion zweiten Grades für einen atmosphärischen und einem Labor Datensatz gezeigt. Die Labordaten zeigen für Skalen $\tau \approx 1000$ einen konstanten Verlauf von S_τ^2 , während ein solcher Verlauf für die atmosphärischen Daten bei keiner Skala zu erkennen ist.

Aufgrund der Problematik der Definition atmosphärischer Windgeschwindigkeiten ist es schwierig, den Einfluss der Turbulenz adäquat zu beschreiben. So stellt sich bei der oftmals verwendeten Definition der Turbulenzintensität $\xi = \sigma/\bar{u}$ erneut die Frage nach der angemessenen Mittelungszeit, die der Bestimmung der Standardabweichung $\sigma = \sqrt{\langle(u')^2\rangle}$ sowie der mittleren Geschwindigkeit \bar{u} zu Grunde liegt.

Das Problem eine geeignete Mittelungszeit zu finden spiegelt sich auch in der Definition einer Windböe wider, deren Auftreten als ein herausragendes Problem für viele meteorologische und technische Anwendungen angesehen werden kann. Neben den allgemeinen, sehr offen gehaltenen Definitionen von Windböen, etwa als *'Abweichung von der mittleren Geschwindigkeit, die durchschnittlich einmal pro Referenz-Periode T überschritten wird'* [21], existiert die Definition eines Böenfaktors $G = u_{max}/\bar{u}$, mit dessen Hilfe sich Böen quantitativ für unterschiedlichste meteorologische und orographische Gegebenheiten vergleichen lassen sollten (e.g. [22], [23]).

Doch auch hier ergibt sich neben der erwähnten Abhängigkeit von Meteorologie und Orographie die Problematik der verwendeten Mittelungszeit. So liegt der

⁴Zeitliche und räumliche Inkremente können bei moderater Turbulenz und langsam variierender mittlerer Geschwindigkeit über die *Taylorhypothese* ineinander umgerechnet werden.

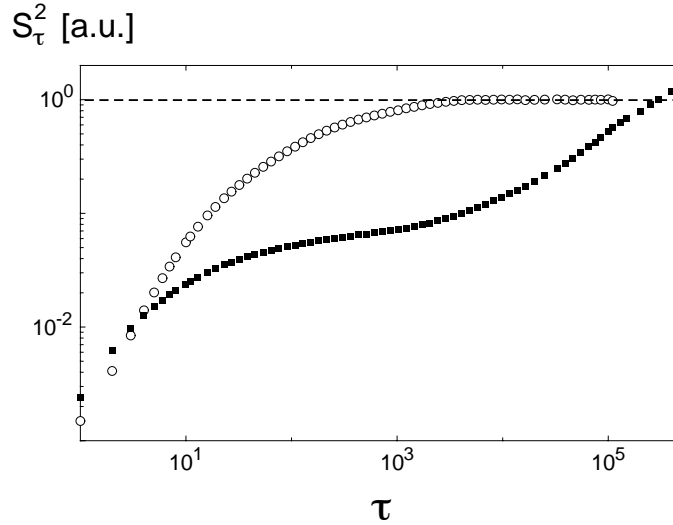


Abbildung 1.1: Dargestellt ist die Strukturfunktion zweiter Ordnung S_τ^2 für einen Labor- (offene Symbole) und einen atmosphärischen Datensatz (geschlossene Symbole) in doppelt-logarithmischer Auftragung. In Kapitel 3 werden beide Datensätze (bezeichnet mit *Lab* und *Off*) vorgestellt. Im Gegensatz zum atmosphärischen Datensatz ist für den Labordatensatz für $\tau > 10^3$ ein klarer Bereich konstanter Strukturfunktionswerte zu erkennen. Für die atmosphärischen Daten entspricht der dargestellte Bereich den Skalen von $0.2s$ bis 10^5s .

Bestimmung der Maximalgeschwindigkeit u_{max} eine Mittelungszeit Δt zugrunde, die mindestens der zeitlichen bzw. räumlichen Integration des verwendeten Anemometers entspricht, oftmals aber auf eine bestimmte Dauer (beispielsweise $3s$) festgesetzt wird. Zur Bestimmung von \bar{u} wird über die Referenzperiode T (zumeist $10min$) gemittelt. Der Böenfaktor hängt dabei stark von Δt bzw. T ab und weist allgemein einen hyperbolischen Verlauf über $\Delta t/T$ auf [24].

Eine detailliertere Klassifikation von Windböen findet sich insbesondere im Bereich technischer Anwendungen wie der Windenergienutzung. In der Norm *IEC 61400-1* wird zwischen fünf unterschiedlichen Böenarten unterschieden⁵: *Extreme operating gusts*, *Extreme direction changes*, *Extreme coherent gusts*, *Extreme coherent gusts with direction change* und *Extreme wind shears*. Die *Extreme operating gust (EOG)* beispielsweise ist definiert durch:

$$u_{Gust,N} = \beta \left(\frac{\sigma}{1 + D/10\Lambda} \right) . \quad (1.7)$$

Dabei bezeichnet σ die Standardabweichung der Geschwindigkeitskomponente in Hauptwindrichtung, D gibt den Rotordurchmesser (einer Windkraftanlage) an, Λ ist ein Skalenparameter (typischerweise $21m$), der Index N bezeichnet die Wiederkehrzeit einer Böe in Jahren und β ist ein Risikoparameter der mit N

⁵Die Abkürzung IEC steht für 'International Electrotechnical Commission'.

ansteigt. Der zeitliche Verlauf der EOG ist ebenfalls definiert und gegeben durch:

$$u(t) = u_0 - 0.37 \cdot u_{Gust,N} \cdot \sin\left(\frac{3\pi}{T}t\right) \left[1 - \cos\left(\frac{2\pi}{T}t\right)\right] . \quad (1.8)$$

T bezeichnet die Böendauer und hängt leicht von der Wiederkehrzeit ab, u_0 ist die Geschwindigkeit vor und nach Durchgang der Windböe. Die anderen vier Definitionen sind im Appendix A zusammengefasst. In Abb. 1.2 ist der zeitliche Verlauf einer EOG Böe wiedergegeben.

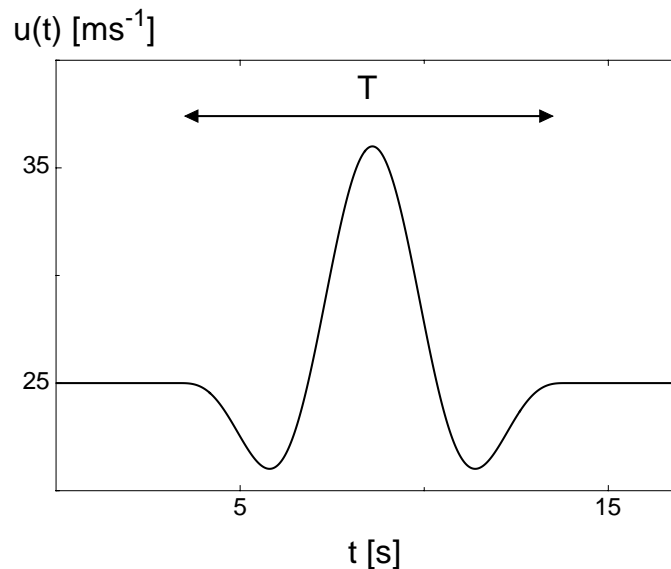


Abbildung 1.2: Dargestellt ist der zeitliche Böenverlauf nach der Norm *IEC 61400-1*. Die Böendauer beträgt $T = 10.5 \text{ s}$ und die Geschwindigkeit vor und nach Durchgang der Böe $u_0 = 25 \text{ ms}^{-1}$. $u_{Gust,N}$ ist mit 14.8 ms^{-1} gegeben.

Ein prinzipieller Schwachpunkt der Charakterisierung von atmosphärischer Turbulenz durch die vorgestellten Beschreibungsgrößen (Turbulenzintensität, Böenfaktor, IEC Definitionen) besteht in der Tatsache, dass hier neben empirischen Faktoren nur die Momente erster und zweiter Ordnung in Form von Mittelwert und Standardabweichung eingehen. Dies ist nur dann ausreichend, wenn atmosphärische Turbulenz vollständig durch eine Gauss-Statistik beschreibbar wäre.

Wie bereits anhand der multifraktalen Eigenschaften turbulenter Geschwindigkeitsfelder verdeutlicht wurde, tritt selbst bei stationärer, homogener und isotroper Turbulenz eine deutlich anomale Statistik der Geschwindigkeitsunterschiede zu Tage. Bei instationärer Turbulenz können selbst die Fluktuationen nicht länger als normalverteilt angenommen werden. Eine vollständige Beschreibung allein durch Mittelwert und Standardabweichung ist deshalb prinzipiell unmöglich. Aus diesem Grund wird atmosphärische

Turbulenz in der vorliegenden Arbeit mit stochastischen Methoden analysiert, die in der Turbulenzforschung etabliert sind und sich nicht auf die ersten beiden Momente beschränken. Im Mittelpunkt steht dabei die Statistik der Geschwindigkeitsinkremente, die sich als natürliches Maß zur Erfassung und Analyse von Windböen erweisen [25].

Das zentrale Ziel der Arbeit ist die Charakterisierung der Inkrement- bzw. Böenstatistik unter besonderer Berücksichtigung der Instationarität des Windes. Zudem wird die Bedeutung der gefundenen anomalen Statistik im Hinblick auf Extremereignisse diskutiert. Diese Thematik wird in den ersten beiden Artikeln behandelt, die in den Kapiteln 2 und 3 zusammengefasst sind.

In einem weiteren Teil der Arbeit steht die Rekonstruktion turbulenter Zeitreihen im Vordergrund, die als Realisationen eines stochastischen Prozesses aufgefasst werden. Dieser Prozess besitzt neben einem deterministischen einen stochastischen Anteil. Der Einfluss des letzteren wird als *dynamisches Rauschen* bezeichnet. Reale Zeitreihen weisen oftmals einen zusätzlichen Rauschanteil auf, der dem Prozess nachträglich überlagert ist und als *Messrauschen* bezeichnet wird. Die Unterscheidung zwischen beiden Rauscharten ist das zentrale Thema des dritten Artikels, der in Kapitel 4 wiedergegeben ist.

Im Folgenden werden die drei im Rahmen dieser Arbeit entstandenen Artikel kurz vorgestellt.

Artikel 1:

F. Böttcher, Ch. Renner, H.-P. Waldl and J. Peinke: 'On the statistics of wind gusts', *Bound.-Layer Meteor.*, 108:163-173, 2003.

Wir zeigen, dass die Inkrementstatistik atmosphärischer Geschwindigkeiten deutlich intermittenter ist als diejenige stationärer, homogener und isotroper Turbulenz. Wird die auf eine mittlere Geschwindigkeit bedingte Statistik betrachtet, verschwinden die Unterschiede weitgehend. In der Wartezeitstatistik von Windböen zeigt sich ein Potenzgesetz, das für Labordaten nicht gefunden wird.

Artikel 2:

F. Böttcher, St. Barth and J. Peinke: 'Small and large scale fluctuations in atmospheric wind speeds', eingereicht in *Stoch. Environ. Res. Risk Assess.*

Der Artikel diskutiert die multifraktalen Eigenschaften von unterschiedlichen atmosphärischen Geschwindigkeitszeitreihen und vergleicht sie mit Zeitreihen aus Laborexperimenten. Es wird ein neues Modell vorgestellt, das die beobachtete Intermittenz als

Überlagerung von stationären Abschnitten homogener und isotroper Turbulenz erklärt. Die Verteilung dieser Abschnitte lässt sich dabei durch eine Weibullverteilung beschreiben.

Artikel 3:

F. Böttcher and J. Peinke: 'A generalized method to distinguish between dynamical and measurement noise in complex dynamical systems', zu veröffentlichen.

Wir zeigen, dass sich Messrauschen anhand eines konstanten, zeitunabhängigen Anteils sowohl beim ersten als auch beim zweiten bedingten Moment offenbart. Die Bedeutung eines solchen *Offsets* der Momente für die Rekonstruktion des deterministischen und stochastischen Anteils der Dynamik wird diskutiert. Für einen Ornstein-Uhlenbeck Prozess kann der Offset quantitativ hergeleitet werden, wodurch sich der gesamte Übergangsbereich von einem reinen Prozess hin zu reinem Rauschen erfassen lässt.

Literaturverzeichnis

- [1] L. F. Richardson. *Weather Prediction by Numerical Process*. Cambridge University Press, 1922.
- [2] A. N. Kolmogorov. The local structure of turbulence in an incompressible viscous flow for very high Reynolds numbers. *Dokl. Acad. Nauk. SSSR*, 305:301–305, 1941.
- [3] A. N. Kolmogorov. A refinement of previous hypotheses concerning the local structure of turbulence in a viscous incompressible fluid at high Reynolds number. *J. Fluid Mech.*, 13:82–85, 1962.
- [4] C. Renner, J. Peinke, and R. Friedrich. Markov properties of small scale turbulence. *J. Fluid Mech.*, 433:383–409, 2001.
- [5] A. N. Kolmogorov. Dissipation of energy in locally isotropic turbulence. *Dokl. Akad. Nauk SSSR*, 32:16–18, 1941.
- [6] G. K. Batchelor. *Fluid Dynamics*. Cambridge University Press, 1994.
- [7] U. Frisch. Turbulence. The legacy of of A. N. Kolmogorov. *Cambridge University Press*, 1995.
- [8] W. D. McComb. *The Physics of Fluid Turbulence*. Oxford University Press, 1996.
- [9] S. B. Pope. *Turbulent Flows*. Cambridge University Press, 2000.
- [10] D. J. Tritton. *Physical Fluid Dynamics*. Oxford University Press, 1998.
- [11] E. J. Fordham. The spatial structure of turbulence in the Atmospheric Boundary Layer. *Wind Engineering*, 90(2):95–133, 1985.
- [12] L. F. Richardson. Atmospheric diffusion shown on a distance-neighbour graph. *Proc. R. Soc. London Ser. A*, 110:709–722, 1926.
- [13] I. van der Hoven. Power spectrum of horizontal wind speed in the frequency range from 0.0007 to 900 cycles per hour. *J. Meteorol.*, 14:160–164, 1957.
- [14] T. Burton, D. Sharpe, N. Jenkins, and E. Bossanyi. *Wind Energy Handbook*. John Wiley and Sons, 2001.
- [15] J. C. Kaimal and J. J. Finnigan. *Atmospheric Boundary Layer Flows*. Oxford University Press, 1994.

-
- [16] R. B. Stull. *An Introduction to Boundary Layer Meteorology*. Kluwer Academic Publ., 1994.
- [17] U. Högström, J. C. R. Hunt, and A.-S. Smedman. Theory and measurements for turbulence spectra and variances in the atmospheric neutral surface layer. *Bound.-Layer Meteor.*, 103:101–124, 2002.
- [18] S. Yahaya, J. P. Frangi, and D. C. Richard. Turbulent characteristics of a semiarid atmospheric surface layer from cup anemometers – effects of soil tillage treatment (Northern Spain). *Ann. Geophysicae*, 21:2119–2131, 2003.
- [19] S. Lovejoy, D. Schertzer, and J. D. Stanway. Direct evidence of multifractal atmospheric cascades from planetary scales down to 1 km. *Phys. Rev. Lett.*, 86(22):5200–5203, 2001.
- [20] E. W. Schulz and B. G. Sanderson. Stationarity of turbulence in light winds during the maritime continent thunderstorm experiment. *Bound.-Layer Meteor.*, 111(3):523–541, 2004.
- [21] L. Kristensen, M. Casanova, M. S. Courtney, and I. Troen. In search of a gust definition. *Bound.-Layer Meteor.*, 55:91–107, 1991.
- [22] J. Wieringa. Gust factors over open water and built-up country. *Bound.-Layer Meteor.*, 3:424–441, 1973.
- [23] H. Ágústsson and H. Ólafsson. Mean gust factors in complex terrain. *Meteorologische Zeitschrift*, 13(2):149–155, 2004.
- [24] Y. Mitsuta and O. Tsukamoto. Studies on spatial structure of wind gusts. *Jour. Applied Meteorol.*, 281:1155–1160, 1989.
- [25] H. Bergström. A statistical analysis of gust characteristics. *Bound.-Layer Meteor.*, 39:153–173, 1987.

Chapter 2

On the Statistics of Wind Gusts

In this article a comparative study of velocity measurements in the free atmosphere and velocity measurements under stationary, local homogeneous and isotropic conditions is made. The probability density functions (PDFs) of atmospheric velocity differences are much more intermittent than those of stationary, homogeneous and isotropic turbulence¹. This directly accounts for an increased probability of observing severe wind gusts. It is shown that atmospheric PDFs become similar to the isotropic ones if they are conditioned on an averaged wind speed value.

Clear differences between isotropic and atmospheric velocity data are found for the waiting time statistics between successive gusts which are defined as velocity differences exceeding a given threshold.

2.1 Introduction

The wind in the atmospheric boundary layer is known to be distinctively turbulent and instationary. As a consequence the wind speed varies rather randomly on many different time scales. These time scales range from long-term variations (years) to very short ones (minutes down to less than a second). The latter are commonly considered to correspond to small-scale (microscale) turbulence. These small-scale fluctuations are superimposed to the mean velocity varying on diurnal or even larger scales. This distinction between a mean flow and superimposed turbulence is justified by the existence of a spectral gap which means that there is only little wind speed variation on time scales between about ten minutes and ten hours [1].

One of the main challenges in turbulence research is the so-called *intermittency of small-scale turbulence*, which corresponds to an unexpected high probability of

¹In the following the term 'isotropic turbulence' instead of 'stationary, homogeneous and isotropic turbulence' will be used.

large velocity fluctuations. (Note that there are also other independent definitions of intermittency related to other phenomena.) For atmospheric winds large velocity fluctuations on small scales correspond to gusts. A more precise statistical description of the occurrences of gusts is important for many applications.

The aim of this paper is to find a possible relation between laboratory turbulence and the atmospheric small-scale one. The mechanisms ruling the atmospheric turbulence are quite complex. Roughly the origins of atmospheric turbulence can be divided into friction and thermal effects. The influence of both generally depends on many different factors like the thermal stability, the topography, the geographical position and so on [2].

In laboratory experiments the situation is less complicated and easier to control. Here turbulence may be generated only by flow disturbances, speed and direction of the mean flow can be kept constant and no buoyancy effects have to be considered. Despite all these differences between different types of turbulence it is a common concept [3] that cascade-like processes lead to universal statistical features of small-scale turbulence.

In this work we analyze two data sets, (a) one from a wake flow behind a cylinder recorded in a wind tunnel and (b) data from atmospheric wind.

(a) The velocity of the laboratory data was measured in the plane that is spanned by the cylinder axis and the mean velocity direction at a great distance (100 times the diameter D of the cylinder, $D = 0.02m$) to the cylinder [4]. At these distances the periodical flow patterns (Karman-street) arising directly beyond the cylinder are vanished and the turbulent wake flow can be considered to be rather isotropic and fully developed. The Reynolds number is $Re = \frac{UD}{\nu} \approx 30000$.

(b) The atmospheric data set we use was recorded near the German coastline of the North Sea in Emden [5]. The velocity was measured by means of an ultrasonic anemometer at 20 m height. The sampling frequency was 4Hz. The measuring period took about one year (1997-1998). The distance to the sea is between some kilometers and a few tens of kilometers - depending on the direction. After careful investigation of the quality of the data we examine a representative 275-hour-excerpt of October 1997 and focus on the velocity component in direction of the mean wind [6]. During this period the velocity was recorded continuously without significant breaks. It is clear that over such a long period meteorological conditions are changing.

In the first part of this paper the statistics of atmospheric wind gusts as a small-scale turbulence phenomenon are examined using the statistics of the horizontal velocity increments. The results are compared to the velocity increments of the laboratory data. In the second part we examine the waiting time distributions of successive wind gusts to resolve their temporal structure. We find evidence that wind gusts are connected to the instationarity of the wind but can be reduced to stationary laboratory turbulence if a proper condition on a constant mean velocity is done.

2.2 Probabilistic Description of Wind Gusts

Due to the large size of atmospheric flow dimensions the atmospheric wind is distinctively turbulent leading to very large Reynolds number Re . Although a characteristic length scale L for atmospheric turbulent flow structures depends on parameters like the surface roughness z_0 or the height z above ground, L may be of the order of about $100m$ [2]. With typical wind speeds of $U \approx 10ms^{-1}$ and more Reynolds numbers of $Re = \frac{UL}{\nu} \geq 10^8$ are obtained.

Turbulent velocity time series are commonly decomposed into a mean speed value $\bar{u}(t)$ and random fluctuations (turbulence) around it $u'(t)$:

$$u = \bar{u} + u' \quad . \quad (2.1)$$

In the following only the component in mean wind speed direction is considered. Thus u' and \bar{u} denote the fluctuating and the averaged part of the wind speed in mean flow direction.

In wind energy research an averaging period of ten minutes is commonly used, even though the smallest possible averaging period is in general time-dependent [7]. In this paper we are interested in the small-scale fluctuations, thus we only need a lower bound of such an averaging time. The presented analysis was performed with different averaging times ranging from one minute up to ten minutes. No significant changes in our results were observed. Thus we proceed with an averaging period of ten minutes.

The larger the fluctuation values u the more turbulent the wind field becomes. In wind energy research this is often expressed by means of the *turbulence intensity* ξ which is defined as the standard deviation σ in relation to the mean velocity \bar{u} [2]:

$$\xi = \frac{\sigma}{\bar{u}} \quad . \quad (2.2)$$

Nevertheless the value of ξ does not contain any dynamical or time-resolved information about the fluctuation field itself.

To achieve a deeper understanding of wind gusts we investigate how far wind gusts are related to the well known features of small-scale turbulence.

As a natural and simple measure of wind gusts we use the statistics of *velocity increments* u_τ :

$$u_\tau = u(t + \tau) - u(t) \quad , \quad (2.3)$$

commonly used for intermittency analysis of small-scale turbulence in laboratory data [4]. The increments directly measure the velocity difference after a characteristic time τ as illustrated in Fig.2.1. So a large increment exceeding a certain threshold S ($u_\tau > S$) can be defined as a gust.

For a statistical analysis we are interested in how frequent a certain increment value occurs and whether this frequency depends on τ . Therefore we first calculate the *Probability Density Functions* (PDFs) $p(u_\tau)$ of the increments of the

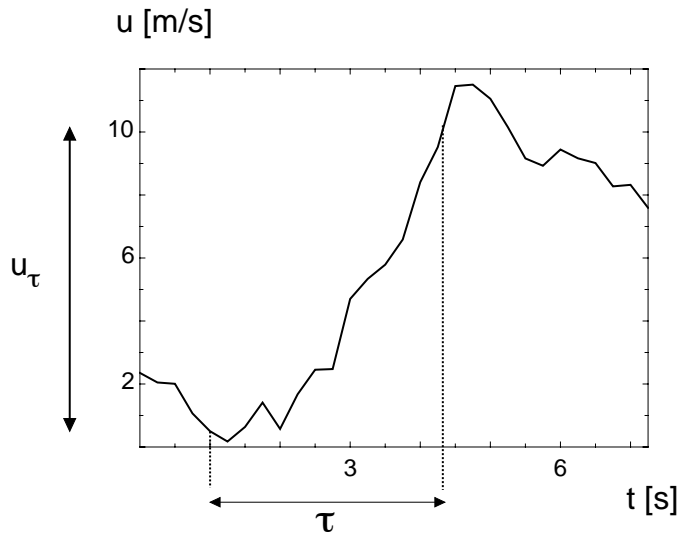


Figure 2.1: The picture shows an arbitrary excerpt of the horizontal wind speed time series including a strong wind gust.

atmospheric velocity fluctuations. In Fig. 2.2 the PDFs for 5 different values of τ are shown. These distributions are all characterized by marked fat *tails* and a peak around the mean value. Such PDFs are called *intermittent* and differ extremely from a *Gaussian distribution* that is commonly considered to be the suitable distribution for continuous random processes.

A Gaussian or *normal* distribution is uniquely defined by its mean value μ and its standard deviation σ . Thus every distribution can be compared to a Gaussian distribution in a quantitative way.

In Fig. 2.3 we compare one of the measured PDFs ($\tau = 4s$) with a normal distribution with the same σ . In this presentation the different behavior of the tails of both distributions becomes evident. Note that the large increments – located in the tails of the PDFs – correspond to strong gusts. For instance the value of $u_\tau = 7\sigma$ corresponds to a velocity ascending of $5.6ms^{-1}$ during $4s$. As shown in Fig. 2.3 (arrow) the measured probability density of the increments of our wind data is about 10^6 times higher than for a corresponding Gaussian distribution! The value 10^6 – for instance – means that a certain gust which is observed about five times a day should be observed just once in 500 years if the distribution were a Gaussian instead of the observed intermittent one.

But intermittent distributions seem to appear quite often in natural or economical systems like in earthquake- [8], foreign exchange market- [9] or even in some traffic-statistics [10].

What kind of statistics do we get in the case of local isotropic and stationary laboratory experiments? The typical PDFs in laboratory turbulence – as shown in Fig. 2.4 a) – change from intermittent ones for small values of τ to

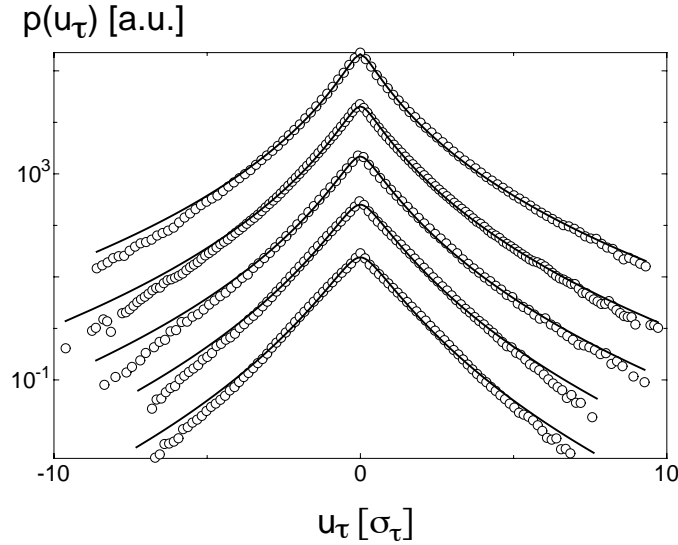


Figure 2.2: The PDFs of the increments of the atmospheric velocity fluctuations (normalized with $\sigma_\tau := \sqrt{u_\tau^2}$) for τ being $0.25s$, $1.0s$, $6.8s$, $32s$ and $2074s$ (full symbols from the top to the bottom) are drawn in. They are shifted in vertical direction against each other for a clearer presentation and the corresponding fits according to Eq. (2.5) are shown as solid curves. $p(u_\tau)$ is given in arbitrary units (a.u.).

rather Gaussian shaped distributions with increasing τ ($\tau \approx T$), where T is the correlation or integral time:

$$T = \int_0^{\infty} R(\tau) d\tau \quad , \quad (2.4)$$

well defined for laboratory data where T is found to be about $6 \cdot 10^{-3}s$. $R(\tau)$ denotes the autocorrelation function of the fluctuations.

For the atmospheric wind data Eq. (2.4) does not converge properly. To fix a large time T we take $1800s$ as the upper limit of the integral and thus obtain $T = 34s$.

For the PDFs of the atmospheric velocity field this characteristic change of shape, even for τ -values higher than $T = 34s$ (as shown in Fig. 2.2) is not observed.

As already mentioned a fundamental difference between atmospheric and laboratory turbulence is that the latter is stationary. In laboratory experiments one usually deals with fixed speed and direction of the mean wind \bar{u} , which is obviously never the case for atmospheric wind fields. Therefore in a second step we calculate the PDFs of the atmospheric velocity increments only for certain mean velocity intervals. That means that only those increments are taken into account with \bar{u} ranging in a narrow velocity interval with a width of typically

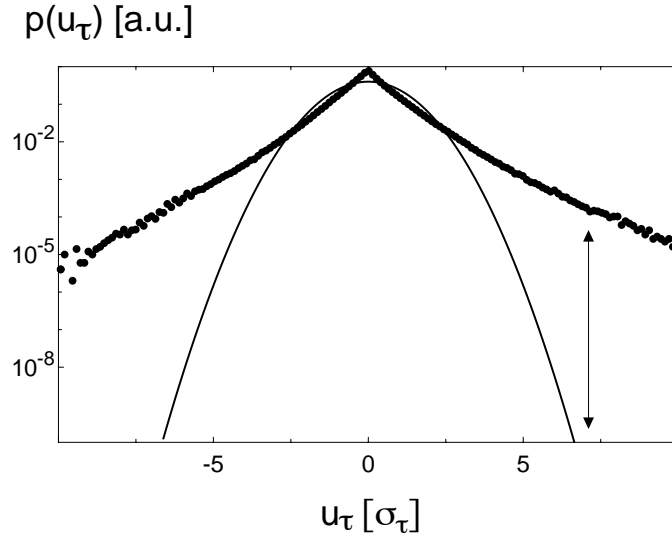


Figure 2.3: The distribution of the increments for $\tau = 4s$ is represented by the symbols, a Gaussian distribution with the same standard deviation σ_τ by the solid line (parabola due to the semilogarithmic presentation). Both distributions are normalized with $\sigma_\tau = 0.8ms^{-1}$.

$1ms^{-1}$. These *conditioned* PDFs $p(u_\tau|\bar{u})$ all show a similar qualitative change of shape like those of the laboratory experiment². This is illustrated in Fig. 2.4 b) for one exemplary mean velocity interval.

To quantify this similarity we use a well established fit by an empirical explicit function for the PDF. This formula was derived in [11] on the basis of Kolmogorov's understanding of a turbulent cascade:

$$p(u_\tau) = \frac{1}{2\pi\lambda_\tau} \int_0^\infty \exp\left[-\frac{u_\tau^2}{2s^2}\right] \cdot \exp\left[-\frac{\ln^2(s/s_0)}{2\lambda_\tau^2}\right] \frac{d(\ln s)}{s} . \quad (2.5)$$

In Fig. 2.2 and Fig. 2.4 these functions are represented by the solid lines. λ_τ^2 is the fundamental parameter in equation (2.5) and determines the shape of the probability distribution. As it can easily be seen equation (2.5) reduces to a Gaussian distribution if λ_τ^2 goes to zero:

$$\lim_{\lambda_\tau^2 \rightarrow 0} p(u_\tau) = \frac{1}{s_0\sqrt{2\pi}} \exp\left[-\frac{u_\tau^2}{2s_0^2}\right] . \quad (2.6)$$

On the other hand the more λ_τ^2 increases the more intermittent the distributions become. In this way the parameter λ_τ^2 may serve to compare the PDFs with each other in a more quantitative way. In Fig. 2.5 the evolution of this parameter as a function of the increment distance τ is shown.

²Only for very small values of \bar{u} ($u < 1ms^{-1}$) this change of shape is not observed.

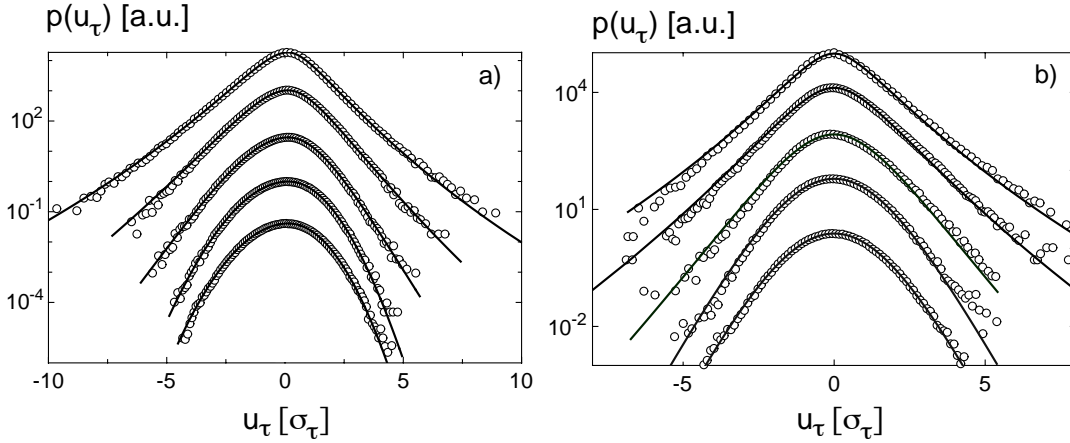


Figure 2.4: **a)** The symbols represent the PDFs $p(u_\tau)$ of the laboratory increments for different values of τ . From the top to the bottom τ/T takes the values: 0.005, 0.02, 0.17, 0.67 and 1.35. **b)** The conditioned PDFs of the atmospheric data are presented, here τ/T is 0.008, 0.03, 0.2, 0.95 and 1.9. The mean wind interval on which the increments are conditioned covers the values between 4.5m s^{-1} and 5.6m s^{-1} . In both cases the solid lines correspond to the fit according to Eq. (2.5). PDFs and fits are shifted in vertical direction against each other for clarity of presentation.

Other laboratory measurements [11], [12] of λ_τ^2 have shown evidence that it saturates at approximately 0.2. As shown in Fig. 2.5 λ_τ^2 of the conditioned wind increments as well as of the laboratory ones is approximately 0.2 for small τ -values. Furthermore it tends to zero with increasing τ . For the atmospheric data none of these two features is observed in the case of the unconditioned increments, λ_τ^2 is rather independent from τ with a value of about 0.7. A constant behavior of λ_τ^2 means that the shape of the PDFs remains unchanged, while its variance may change.

Thus we have shown that the anomalous statistics of wind fluctuations on discrete time intervals – which are obviously related to wind gusts – can be reduced to the well known intermittent (anomalous) statistics of local isotropic turbulence. This result deviates from results of wind data reported in [13], where it is claimed that their unconditioned wind PDFs behave like those from laboratory measurements.

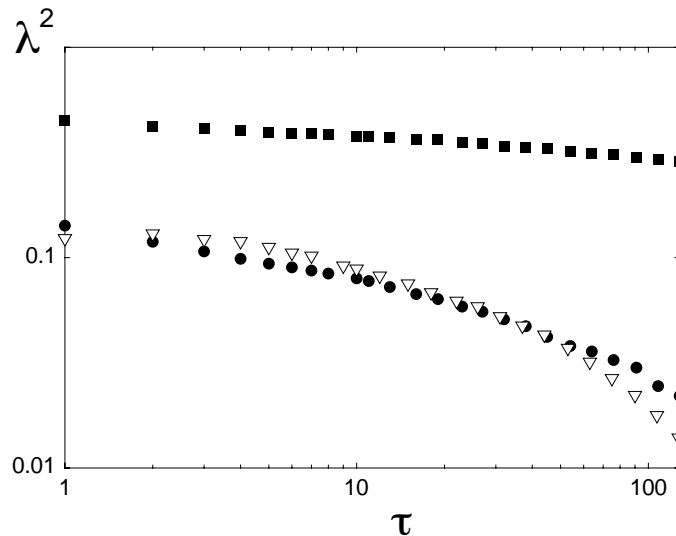


Figure 2.5: λ_τ^2 as a function of the increment distance τ is shown for the PDFs of the laboratory data (open symbols) and of the unconditioned (squares) as well as for the wind data conditioned on the mean velocity interval $[4.5; 5.6]ms^{-1}$. The axes both are logarithmic. For the laboratory data $\tau = 1$ corresponds to $10^{-5}s$ and for the wind data to $0.25s$.

2.3 Waiting Time Distribution

So far we have shown how the atmospheric turbulence is related to the laboratory one in a statistical way. This probabilistic approach describes the frequency with which certain gusts occur but it is not clear how they are distributed in time. In this sense we now examine the waiting times between successive wind gusts.

The marked fat tail behavior of the unconditioned PDFs – as illustrated in Fig. 2.2 – points at an interesting effect. In [14] the equivalence between the divergence of the moments $\langle x^q \rangle$ and the hyperbolic (intermittent) form of PDFs which leads to a power law behavior of the probability distribution is emphasized:

$$p(x \geq S) \propto S^{-q} \quad , S \gg 1 \quad . \quad (2.7)$$

A famous example of such a natural power law behavior is the *Gutenberg-Richter-law* [15] that describes the frequency N of earthquakes with a magnitude being greater than a certain threshold M (magnitude):

$$\begin{aligned} \log(N(m \geq M)) &= a - bM \\ \Leftrightarrow N(m \geq M) &\propto 10^{-bM} \quad . \end{aligned} \quad (2.8)$$

But also the waiting time distribution of fore- and after shocks obey a power-law, what is known as the *Omori-law* [16].

In this sense we now examine the waiting time distribution of wind gusts. Therefore we refer to the gust illustrated in Fig. 2.1 choosing different thresholds

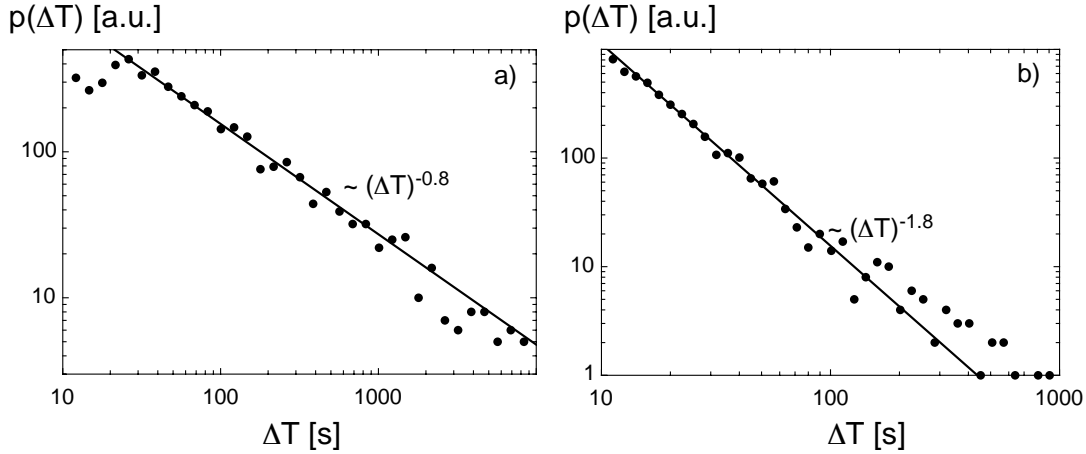


Figure 2.6: The filled symbols illustrate the waiting time distributions $p(\Delta T)$ – given in arbitrary units – between successive gusts. Additionally two power-law functions are fitted to the measured values (solid lines).

a) The distance is $\tau/T = 0.3$ and the threshold is set to be $S = 4.0ms^{-1}$. The exponent is found to be -0.8 .

b) The distance is $\tau/T = 2.0$ and the threshold is set to be $S = 1.5ms^{-1}$. The exponent is found to be -1.8 .

S and different increment distances τ (see Eq. (2.3)). Always when the condition $u_\tau > S$ is fulfilled a gust event is registered.

The waiting time distributions $p(\Delta T)$ for $S = 4.0ms^{-1}$ and $\tau = 10s$ and for $S = 1.5ms^{-1}$ and $\tau = 65s$ are shown in Fig. 2.6 a) and 2.6 b), respectively. Due to the double-logarithmic presentation both distributions follow a power law but with different exponents. The exponents depend on S and τ . This power law behavior of the waiting time distributions is only observed for the atmospheric wind data and not for the stationary laboratory one.

2.4 Discussion and Summary

On the basis of well defined velocity increments an analogous analysis of measured wind data and measured data from a turbulent wake was performed. The statistics of velocity increments, as related to the occurrence frequency of wind gusts, showed that they are highly intermittent. These anomalous (not Gaussian distributed) statistics explain an increased high probability of finding strong gusts. This could be set in analogy with turbulence measurements of an idealized, local isotropic laboratory flow if a proper condition on a mean wind speed was performed. This result is rather astonishing, insofar as solely the condition on the mean velocity leads to a good agreement between the PDFs of the wind velocity increments and those of the laboratory wake flow. At least for our data

it seems to be not necessary to introduce further conditions which take special meteorological situations into account. A possible explanation is the proposed universality of small-scale turbulence which means that the statistics of the small-scale fluctuations become independent of the driving large scale structures.

As a further statistical feature of wind gusts we have investigated the waiting times between successive gusts exceeding a certain strength. Here we find power-law-statistics (fractal statistics) – similar to earthquake statistics – that can not be reproduced in laboratory measurements.

To conclude we have shown two important aspects of wind gusts. The overall occurrence statistics could be set into analogy to the anomalous statistics of velocity increments in local isotropic turbulence. The time structure of successive gust events displays fractal behavior. We think that these results may be helpful for a better characterization and understanding of gust events.

Of course we have to note that these results are obtained from one single wind data set. It should be very interesting to explore not only the effect of conditioning on a mean wind velocity but also on different flow situations or different boundary layer or other environmental conditions.

Bibliography

- [1] E. Hau. *Windturbines: Fundamentals, Technologies, Application, and Economics*. Springer, 2000.
- [2] T. Burton, D. Sharpe, N. Jenkins, and E. Bossanyi. *Wind Energy Handbook*. John Wiley and Sons, 2001.
- [3] U. Frisch. Turbulence. The legacy of of A. N. Kolmogorov. *Cambridge University Press*, 1995.
- [4] St. Lück. *Skalen aufgelöste Experimente und statistische Analysen von turbulenten Nachlaufströmungen*. PhD thesis, Carl-von-Ossietzky University of Oldenburg, 26111 Oldenburg, Germany, 2000.
- [5] H. Hohlen and J. Liersch. Synchrone Messkampagnen von Wind- und Windkraftanlagen am Standort FH Ostfriesland, Emden. *DEWI Magazin*, 12:66–74, 1998.
- [6] F. Böttcher, C. Renner, H.-P. Waldl, and J. Peinke. Problematik der Windböen. *DEWI Magazin*, 2001.
- [7] G. Trevino and E. L. Andreas. Averaging intervals for spectral analysis of nonstationary turbulence. *Bound.-Layer Meteor.*, 95(2):231–247, 2000.
- [8] D. Schertzer and S. Lovejoy. Multifractal generation of Self-Organized Criticality. *Fractals Nat. Appl. Sci.*, A-41:325–339, 1994.
- [9] S. Ghashghaie, W. Breymann, J. Peinke, P. Talkner, and Y. Dodge. Turbulent cascades in foreign exchange markets. *Nature*, 381:767–770, 1996.
- [10] J. C. Vassilicos. Turbulence and Intermittency. *Nature*, 374:408–409, 1995.
- [11] B. Castaing, Y. Gagne, and E. J. Hopfinger. Velocity probability density functions of high Reynolds number turbulence. *Physica D*, 46(2):177–200, 1990.
- [12] B. Chabaud, A. Naert, J. Peinke, F. Chilla, B. Castaing, and B. Hébral. Transition toward developed turbulence. *Phys. Rev. Lett.*, 73(24):3227–3230, 1994.
- [13] M. Ragwitz and H. Kantz. Indispensable finite time corrections for Fokker-Planck equations from time series data. *Phys. Rev. Lett.*, 87(25):254501, 2001.

- [14] D. Schertzer and S. Lovejoy. *Nonlinear Variability in Geophysics 3*. Lecture Notes, Cargèse, 1993.
- [15] B. Gutenberg and C. F. Richter. Earthquake magnitude, intensity, energy and acceleration. *Bull. Seismol. Soc. Am.*, 46:105–143, 1956.
- [16] F. Omori. On the aftershocks of earthquakes. *J. Coll. Sci. Imp. Univ. Tokyo*, 72:111, 1894.

Chapter 3

Small and Large Scale Fluctuations in Atmospheric Wind Speeds

In this article atmospheric wind speeds and their fluctuations at different locations (onshore and offshore) are examined. One of the most striking features is the marked intermittency of probability density functions (PDF) of velocity differences – no matter what location is considered. The shape of these PDFs is found to be robust over a wide range of scales which seems to contradict the mathematical concept of stability where a Gaussian distribution should be the limiting one.

Motivated by the instationarity of atmospheric winds it is shown that the intermittent distributions can be understood as a superposition of different subsets of stationary, homogeneous and isotropic turbulence. Thus we suggest a simple stochastic model to reproduce the measured statistics of wind speed fluctuations.

3.1 Introduction

Atmospheric wind may be seen as a prime example of a turbulent velocity field with very high Reynolds numbers of about $Re \approx 10^8$ [1]. Reynolds numbers as large as this prevent analytical calculations and direct numerical simulations. Therefore the flow has to be described in a statistical way. For the estimation of extreme loads as well as for risk estimations the statistics of velocity fluctuations $u'(t)$ and velocity differences should be known¹. It has been shown that these

¹In the following we only consider the wind speed components in mean wind speed direction instead of the vectorial velocity.

statistics obey non-Gaussian, intermittent distributions (e.g. [2], [3]) that directly correspond to an increased number of wind gusts [4].

Nevertheless, for most technical and meteorological problems fluctuations as well as fluctuation differences are assumed to obey Gaussian statistics. Therefore simulations of atmospheric velocities are often based on Gaussian processes [5].

Fluctuation differences are commonly measured using *velocity increments*:

$$u_\tau(t) := u(t + \tau) - u(t) \quad . \quad (3.1)$$

Large increment values can be identified as wind gusts as long as the time step τ is rather small. The demand for a small τ -value (typically less than a minute) is due to the fact that gusts are related to large velocity rises during short times. Rises that occur over time steps of several hours – for instance – are not called wind gusts but large scale variations.

The difficulty to fix a suitable time scale mirrors the fact that atmospheric winds exhibit variations on any time scale – in principle ranging from seconds (and less) up to centuries. For most practical applications, such as engineering and meteorology one mainly distinguishes between large scale variations such as diurnal, weekly and seasonal changes and variations on small scales often referred to as *atmospheric turbulence* or *gustiness* [1]. The existence of a *mesoscale gap* as proposed by [6] which divides small (micro) and large (macro) scales in a more rigorous way has strongly been debated in recent years (e.g. [7], [8]).

In this paper we focus on the scale dependent statistics of atmospheric increments and compare them to that of homogeneous, isotropic and stationary turbulence² as realized in laboratory experiments. For isotropic turbulence the statistical moments of increments, the so-called structure functions have been intensively studied [9]. Their functional dependence on the scale τ is described by a variety of multifractal models. Besides the analysis of moments, probability density functions (PDFs) are often considered. These show a transition from Gaussian distributions to intermittent (heavy-tailed) ones as scale decreases. Unfortunately the analysis of moments as well as that of probability density functions $p(u_\tau)$ is more or less restricted to the *inertial range* – the range of scales larger than the Taylor scale Θ (where dissipation effects become significant) and smaller than the integral scale³ T .

The challenge is to describe and to explain the measured fat-tailed distributions and the corresponding non-convergence to Gaussian statistics. Large increment values in the tails directly correspond to an increased probability⁴

²In the following the term 'isotropic turbulence' instead of 'homogeneous, isotropic and stationary turbulence' will be used.

³Normally Θ and T denote length scales. For constant mean velocities and applying Taylor's hypothesis of frozen turbulence length- can be defined as time-scales as well. Here we will proceed with corresponding time scales.

⁴The probability to observe an increment $u_\tau \in [u_\tau, u_\tau + du_\tau]$ is just given by $p(u_\tau)du_\tau$.

(risk) to observe large and very large events (gusts). As pointed out in [10] the probability to observe large events – e.g. events twice as large as a reference – can become negligible for a Gaussian while for heavy-tailed distributions there is still a significant probability to observe it.

The atmospheric PDFs – we examine here – differ from those of turbulent laboratory flows where – with decreasing scale – a change of shape of the PDFs is observed (e.g. [11]). For large scales the distributions are Gaussian while for small scales they are found to be intermittent. The atmospheric PDFs however change their shape only for the smallest and then stay intermittent for a broad range of scales. Such a constant shape for larger and larger scales is expected only for stable distributions such as Gaussian ones or the Lévy stable laws [12]. Although the decay of the tails indicates that distributions should approach Gaussian ones (as for isotropic turbulence) they show a rather robust exponential-like decay. This point will be clarified in chapter 3.3.2.

In chapter 3.3.1 and 3.3.2 it will be shown that atmospheric increments behave quite similar to those of isotropic turbulence for small scales but differ significantly for large ones. We therefore introduce a model – chapter 3.4 – that interprets atmospheric increment statistics as a large scale mixture of subsets of isotropic statistics. When mixing is weak the same statistics as for isotropic turbulence are recovered while for strong mixing robust intermittency is obtained. In chapter 3.5 the results are briefly discussed.

3.2 The Data

The analysis presented in the following is based on one laboratory and four different atmospheric data sets. In addition to accessibility reasons the latter were chosen in such a way that their environmental and meteorological characteristics differ significantly. Therefore one offshore and three onshore data sets are examined. Additionally a laboratory data set was chosen as an example of an approximately isotropic turbulent wake-flow.

The first data set was recorded in October 1997 near the German coastline of the North Sea in Emden at a height of 20m by means of an ultrasonic anemometer [13]. The wind speed was measured continuously over a period of 275 hours. In the following this data set will be referred to as *On1*.

The second data set – denoted as *On2* – was obtained from a hot-wire measurement 6m above the ground (in flat terrain) [14]. Here the wind speeds of approximately one hour were considered.

On3 – the third data set was recorded in a very complex terrain near Oberzeiring (1900m above the sea level) in Austria in 2001 [15]. The velocity was measured by means of an ultrasonic anemometer. The data consists of 255 non-successive blocks of 4 hours length. The choice was made in order to obtain complete and continuous data within each block.

The fourth data set – referred to as *Off* – was recorded during an offshore measuring campaign at Roedsand in the Danish Baltic Sea at 30m height between 1998 and 1999 [2]. From this period 58 non-successive days were chosen. Again the choice was made in order to obtain complete and continuous data for each day.

The laboratory data – denoted as *Lab* – were obtained from a wake flow measurement in the wind tunnel of Erlangen in 1998 [16]. A hot-wire was located 2m behind a cylinder of diameter $D = 0.02m$ in the plane spanned by the cylinder axis and the mean velocity direction. Here the turbulent flow can be considered to be locally isotropic and fully developed. With a mean velocity of $\bar{u} = 20.9ms^{-1}$ a Reynolds number of $Re = \bar{u}D\nu^{-1} \approx 30,000$ is obtained. Taylor and integral scale are found to be $\Theta \approx 2 \cdot 10^{-4}s$ and $T \approx 6 \cdot 10^{-3}s$, respectively.

For atmospheric data sets it is difficult to define an integral scale T because of the instationarity of atmospheric velocities that causes very long-range correlations $R(\tau) \propto \langle u(t+\tau)u(t) \rangle$ so that the integral time

$$T := \int_0^{\infty} R(\tau) d\tau \quad (3.2)$$

cannot be estimated properly. Only for *On2* an estimate of the integral time can be given because of the rather constant flow conditions during the short measuring period of about 1 hour.

For *On2* the Taylor scale Θ can be calculated while for all other atmospheric data sets the sampling frequency is too low for Θ to be resolved.

In Table 3.1 a short overview of the most important specifications of all five data sets is given.

	On1	On2	On3	Off	Lab
N [1]	3,958,874	20,480,000	14,688,000	25,056,000	12,500,000
blocks [1]	1	1	255	58	100
f [Hz]	4	5,000	4	5	100,000
\bar{u} [ms^{-1}]	3.4	8.3	6.6	9.6	20.9
min [ms^{-1}]	0.0	0.8	0.02	0.6	15.9
max [ms^{-1}]	18.1	18.1	39.0	36.1	25.5
$\bar{\sigma}$ [ms^{-1}]	1.7	2.3	4.2	3.2	1.1
Θ [s]	< 0.25	≈ 0.01	< 0.25	< 0.2	$\approx 2 \cdot 10^{-4}$
T [s]	–	≈ 14	–	–	$\approx 6 \cdot 10^{-3}$

Table 3.1: The table summarizes some characteristic values of the different data sets, from top to bottom these are number of data points N , number of blocks, sample frequency f , mean velocity \bar{u} , minimum, maximum, average standard deviation $\bar{\sigma}$, Taylor scale Θ and integral scale T .

3.3 Analysis

3.3.1 Scaling in Isotropic and Atmospheric Turbulence

The central assumption for turbulent velocity time series is that they have a self-similar structure (a direct consequence of scale invariance of the Navier Stokes Equation) in the *inertial range*. This means that within this range the disorder of velocity fluctuations has a similar structure on every scale but with a scale-dependent magnitude. To quantify this one usually calculates the (absolute) moments of increments

$$S_\tau^n = \langle |u_\tau|^n \rangle \quad , \quad (3.3)$$

which are also called *structure functions* of order n . Instead of calculating the absolute moments one can also consider $\langle u_\tau^n \rangle$ (see [17] for a more detailed discussion).

In isotropic turbulence structure functions are assumed to scale as:

$$S_\tau^n \propto \tau^{\zeta_n} \quad . \quad (3.4)$$

A linear (monofractal) scaling exponent ζ_n corresponds to a self-similar structure as proposed by Kolmogorov in 1941 [18] who found that the scaling exponent should be

$$\zeta_n = \frac{n}{3} \quad (3.5)$$

due to dimensional reasons. Instead of this linear behavior various experiments suggest that the scaling exponent is a non-linear function of n . In 1962 Kolmogorov [19] introduced the following non-linear (multifractal) exponent

$$\zeta_n = \frac{n}{3} + \frac{\mu}{18}(3n - n^2) \quad (3.6)$$

motivated by the model of a turbulent cascade with a lognormally distributed energy transfer rate. The parameter μ is called intermittency correction and is found to be close to 0.25 [20] which corresponds to $\zeta_6 = \frac{n}{3} - \mu = 1.75$. This is in agreement with the examined data sets where ζ_6 takes values between 1.67 and 1.80 as shown in Fig. 3.1 a).

In [21] another formula was proposed which seems to fit experimental data slightly more accurately than Eq. (3.6):

$$\zeta_n = \frac{n}{9} + 2 - 2 \left(\frac{2}{3} \right)^{n/3} \quad . \quad (3.7)$$

There are other models besides these two multifractal ones, e.g. [7], [22]. The differences in ζ_n in all these models are rather small (at least for small orders)

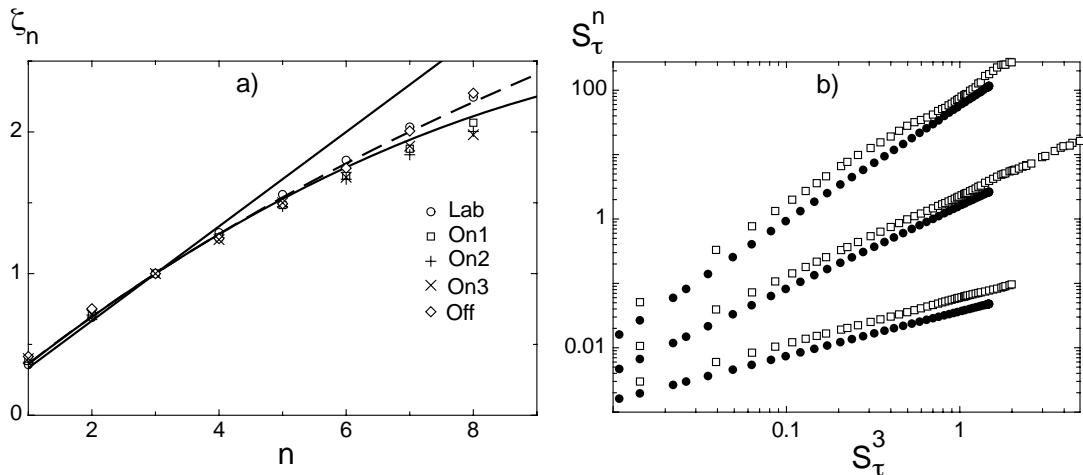


Figure 3.1: **a)** This plot shows the scaling exponents ζ_n as a function of order n for all five data sets. Additionally the linear scaling law given by Eq. (3.5) (straight line) and the non-linear laws according to Eq. (3.6) (curved line) and Eq. (3.7) (curved dashed line) are shown. **b)** The structure functions of order 2, 4 and 6 are plotted against that of order 3 in a double-logarithmic presentation (vertically shifted for clarity of presentation). The open symbols belong to *On1*, the filled ones to *Lab*.

so for simplicity we will restrict following discussions to the models given by Eq. (3.6) and Eq. (3.7).

To estimate the dependence of ζ_n on n one has to calculate ζ_n first. The most common way to do this is to plot $\log(S_\tau^n)$ against $\log(S_\tau^3)$ – a method referred to as Extended Self Similarity (ESS) [23]. The slope of the resulting line is equal to ζ_n . This is shown in Fig. 3.1 b) exemplary for data sets *On1* and *Lab*. In both cases the slopes are in quite good agreement with Eq. (3.6) and Eq. (3.7). The slopes of *On1* show small deviations from linear behavior for large values. These correspond to large scales τ that might not belong to the inertial range anymore. This already indicates that care should be taken when transferring standard analysis of isotropic to atmospheric turbulence.

The difference between isotropic and atmospheric turbulence statistics become more obvious when calculating the flatness F . Assuming inertial range scaling according to Eq. (3.3) and (3.4) the flatness should scale as well and is given by:

$$F := \frac{\langle u_\tau^4 \rangle}{\langle u_\tau^2 \rangle^2} \propto \tau^{\zeta_4 - 2\zeta_2} . \quad (3.8)$$

If Eq. (3.6) is a suitable description⁵ the flatness scales according to:

$$F \propto \tau^{-4\mu/9} , \quad (3.9)$$

⁵Eq. (3.7) and other multifractal models yield very similar results because such low-order exponents as ζ_4 and ζ_2 are quite indistinguishable from each other.

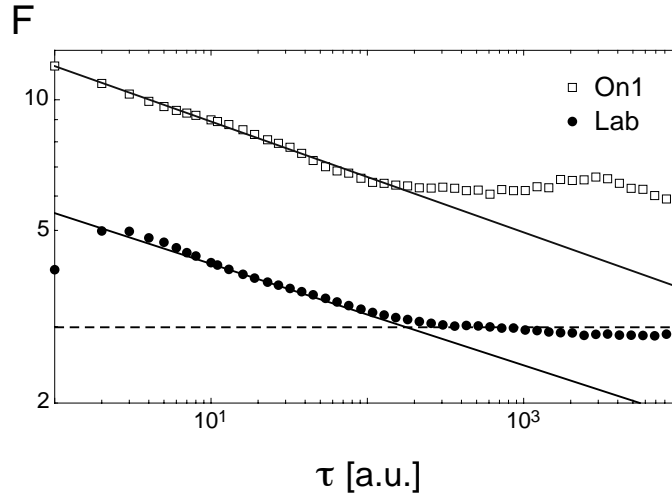


Figure 3.2: The open symbols show the flatness F of *On1* as a function of scale with $\tau = 0.25s$. The filled symbols represent the flatness of *Lab* with $\tau = 0.002T \approx 10^{-5}s$. Additionally fits according to Eq. (3.9) (straight lines) are drawn in with $\mu = 0.29$ (*On1*) and $\mu = 0.26$ (*Lab*). The horizontal dashed line marks $F = 3$ (as for a Gaussian distribution).

as is easily shown inserting Eq. (3.6) into Eq. (3.8). As shown in Fig. 3.2 the measured flatness of the data shows this scaling behavior but the absolute values of F are very different for different data sets. While for the *Lab* data set flatness approaches $F \approx 3$ for large τ it saturates at $F \approx 6$ for the *On1* data set. The flatness of *On3* and *Off* saturates at $F \approx 5$ while for *On2* it goes down to 3.5.

Calculating the flatness of a variable x is often done to estimate the shape of the PDF $p(x)$. A Gaussian distribution has flatness 3. Deviations from this value can be taken as a hint for a non-Gaussian shape of PDFs. In the following the increment PDFs of the given data sets will be examined.

3.3.2 Probability Density Functions in Turbulence

Alternatively to the analysis of scaling exponents one can directly investigate the PDFs of velocity increments $p(u_\tau)$. The scaling behavior as well as all moments (including derived quantities such as flatness or skewness) are immediately given if the distributions on every scale are known.

In principle the knowledge of all moments S_τ^n and the knowledge of the PDFs should contain the same information as can be seen by means of the characteristic function $\varphi(k)$ – which is the Fourier transform of the PDF – defined as:

$$\varphi(k) := \sum_{n=1}^{\infty} S_\tau^n \frac{(ik)^n}{n!} . \quad (3.10)$$

Nevertheless the relation between moments and PDFs is not unique. In [12] it is pointed out that two different PDFs can have exactly the same moments.

From many experiments of isotropic turbulence it is well known that the shape of a PDF changes with scale. Going from larger to smaller scales the distributions become more and more heavy-tailed while for $\tau \geq T$ a Gaussian distribution is obtained. This scale-dependent shape corresponds to non-linear scaling exponents – as introduced in Eq. (3.6) and Eq. (3.7) – while a linear behavior $S_\tau^n = a_n \tau^{\alpha n} = a_n \beta^n$ according to Eq. (3.5) leads to a constant shape. This can be seen by means of the characteristic function in Eq. (3.10) that stays the same for a linear exponent only k is rescaled according to $\tilde{k} = \beta k$.

The analysis of scaling exponents thus focusses on the change in shape of distributions while the shape itself is of minor interest and could even be determined wrongly as shown at the end of the last chapter. Therefore we will henceforth focus on the analysis of PDFs.

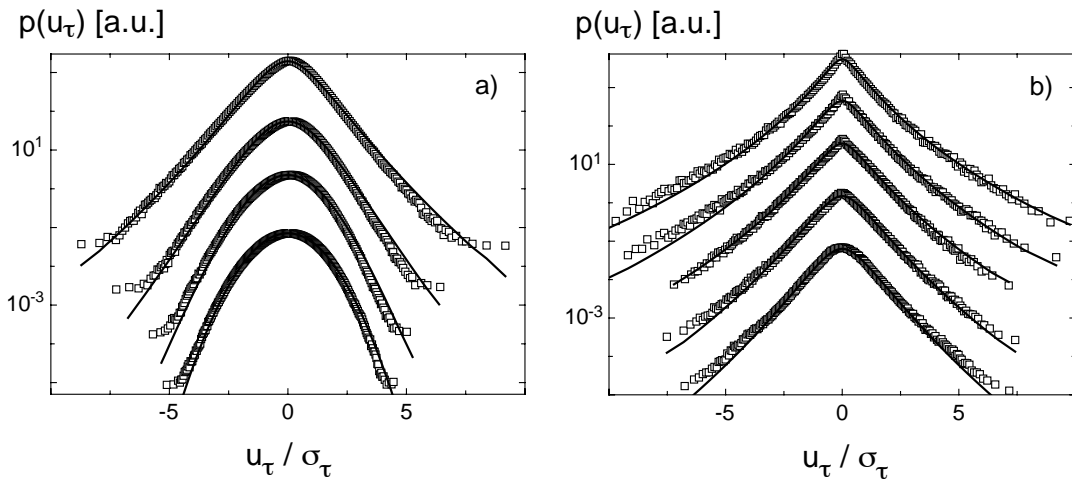


Figure 3.3: **a)** Symbols represent normalized PDFs (with their scale-dependent standard deviation $\sigma_\tau = \sqrt{\langle u_\tau^2 \rangle}$) of the *Lab* data set. From top to bottom τ takes the values: $0.01T$, $0.05T$, $0.2T$ and $1.0T$ where $T \approx 0.006s$ denotes the integral time. **b)** Symbols represent normalized PDFs of the atmospheric data set *On1* with $\tau = 0.5s$, $2.5s$, $25s$, $250s$ and $4000s$. All graphs – in a) and b) – are plotted in a semi-logarithmic presentation and are shifted against each other in vertical direction for clarity of presentation. The solid lines correspond to a fit of the distributions according to Eq. (3.11).

In accordance with Eq. (3.6) (that was derived from the assumption of a log-normally distributed energy transfer rate) B. Castaing et al. [11] introduced a model in which the increment distribution $p(u_\tau)$ is interpreted as a superposition of Gaussian ones $p(u_\tau|\sigma)$ with standard deviation σ . The standard deviation itself is distributed according to a lognormal distribution $f(\sigma)$. The increment

distribution thus reads

$$\begin{aligned} p(u_\tau) &= \int_0^\infty d\sigma \, p(u_\tau|\sigma) \cdot f(\sigma) \\ &= \int_0^\infty d\sigma \frac{1}{\sigma\sqrt{2\pi}} \exp\left[-\frac{u_\tau^2}{2\sigma^2}\right] \cdot \frac{1}{\sigma\lambda\sqrt{2\pi}} \exp\left[-\frac{\ln^2(\sigma/\sigma_0)}{2\lambda^2}\right] \end{aligned} \quad (3.11)$$

and will henceforth be referred to as the *Castaing distribution*. (It is also possible to take distributions different to the log-normal one – see Appendix B.)

Two parameters enter this formula, namely σ_0 and λ^2 . The first is the median of the lognormal distribution, the second its variance. The latter determines the form (shape) of the resulting distribution $p(u_\tau)$ and is therefore called *form parameter*. On one side the larger λ^2 becomes the broader the lognormal distribution and the broader the range of σ that contributes to the integral in Eq. (3.11). On the other side the range of σ becomes smaller and smaller with decreasing form parameter. In the limit of vanishing λ the lognormal becomes a delta distribution

$$\lim_{\lambda \rightarrow 0} \left(\frac{1}{\sigma\lambda\sqrt{2\pi}} \exp\left[-\frac{\ln^2(\sigma/\sigma_0)}{2\lambda^2}\right] \right) = \delta(\sigma - \sigma_0) \quad , \quad (3.12)$$

so that $p(u_\tau)$ is reduced to a Gaussian distribution with variance σ_0^2 .

With a proper choice of the form parameter the PDFs $p(u_\tau)$ can well be fitted as it is shown in Fig. 3.3 a) and Fig. 3.3 b). In Fig. 3.3 a) – where the *Lab* data set is presented – the expected change of shape from intermittent to Gaussian distributions with increasing scale is clearly seen.

In contrast to this behavior the PDFs of *On1* in Fig. 3.3 b) look totally different. They are much more intermittent and do not approach a Gaussian distribution even for very large scales. For scales larger than about $25s$ the shape remains rather constant. This is in accordance with the finding of the slow decrease of flatness shown in Fig. 3.2 because in the lognormal model flatness is linked to the form parameter [24] according to

$$\lambda^2 \propto \ln\left(\frac{F}{3}\right) \quad . \quad (3.13)$$

In this sense constant flatness larger than 3 corresponds to constant λ^2 larger than 0 and thus to rather scale-independent intermittent distributions as shown in Fig. 3.3 b) exemplary for the *On1* data set. The λ^2 -values for all data sets are illustrated in Fig. 3.4 revealing a weak scale-dependence for *On1*, *On3* and *Off* and a large one for *On2* and *Lab*.

In isotropic turbulence scale-independent distributions are also found when the scales are larger than the integral time T . In this case the distributions

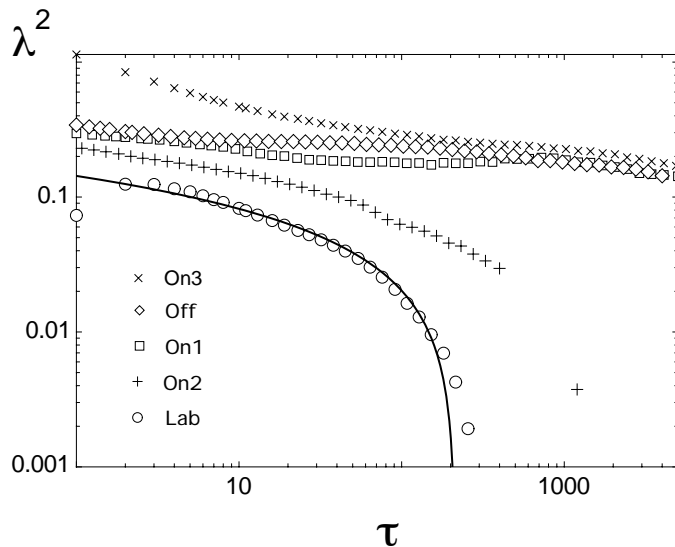


Figure 3.4: The form parameter for the data sets *On3*, *On1*, *Off*, *On2* and *Lab* are shown in double-logarithmic presentation. In that order $\tau = 1$ corresponds to 0.25s, 1s, 1s, 0.02s and 10^{-5} s ($0.002T$). The solid line represents a fit according to Eq. (3.23).

are always Gaussian [25]. Such *stable* Gaussian PDFs can be seen as the result of a stochastic Gaussian process. The other class of stable distributions are the so-called Lévy distributions – characterized by power-law tails – which can be obtained from a fractional stochastic process. The observed atmospheric increment PDFs show robust (stretched) exponential tails that decay faster than a power-law and slower than a Gaussian distribution. So the question arises whether the atmospheric PDFs can be explained as a fractional process or as a superposition of different Gaussian processes in analogy to the *Castaing distribution*. To decide this the concept of stability and the connection to increment analysis should briefly be introduced.

3.3.3 Stable Distributions

Consider the sum $s_m = \sum_i^m x_i$ of m independent and identical distributed (i.i.d.) variables. The distribution of the variable x is denoted with p and that of the sum-variable by \hat{p} . The distribution p (or \hat{p} respectively) is then called *stable* if for large m ($m \rightarrow \infty$)

$$\hat{p}(x') dx' = p(x) dx \quad \text{with} \quad x' = Ax + B \quad (3.14)$$

is fulfilled [12]. This means that for sufficiently large m the shape of the distribution does not change as m increases.

Transferred to increment analysis an increment over a scale τ can be identified as variable x and the increment of a larger scale $m\tau$ as the sum-variable s_m . It is immediately shown that

$$u_{m\tau}(t) = \sum_{i=0}^{m-1} u_{\tau}(t + i\tau) \quad , \quad (3.15)$$

which means that a large increment can be expressed as the sum of smaller ones. When the PDFs of large and small increments are the same this indicates a stable PDF.

The most famous stable distribution is the Gaussian one. Beside this P. Lévy [26] showed that there exists a whole class of stable distributions. Restricting to symmetric distributions their characteristic functions read:

$$\varphi(k) = \exp [i\gamma k - c|k|^\alpha] \quad ; 0 < \alpha \leq 2. \quad (3.16)$$

For asymmetric distributions the characteristic function becomes more complicated (e.g. [27]). The analytical form of the corresponding PDFs is only known for some special cases (e.g. for $\alpha = 1$ it is the Cauchy distribution) but their asymptotic behavior is always known and given by:

$$p(x) \propto C |x|^{-(1+\alpha)} \quad ; x \gg 1 \quad . \quad (3.17)$$

This algebraic decay of tails means that all higher order moments larger than order α do not exist. Generally, distributions with tails decaying faster than $\propto |x|^{-3}$ (defined variance) can only converge to a Gaussian while slower decaying tails indicate that they can only converge to a Lévy stable law.

As already mentioned the examined atmospheric PDFs show a faster than algebraic decay (compare Fig. 3.3 b) and Fig. 3.8 a), b), c), d)) so it is expected that they converge to Gaussian statistics for large scales. Therefore the observed robust intermittency should be explained by mixing different Gaussian distributions rather than by a fractional stochastic process.

3.4 Superposition Model for Atmospheric Turbulence

In [4] it was proposed to take the instationarity of long atmospheric time series into account. In this sense the observed intermittent form of PDFs for all examined scales are found to be the result of mixing statistics belonging to different flow situations. These are characterized by different mean velocities as schematically illustrated in Fig. 3.5. When the analysis by means of increment statistics is conditioned on periods with constant mean velocities results are found to be very similar to those of isotropic turbulence. This can be set in analogy to the *Castaing distribution* that interprets intermittent PDFs as a superposition of intervals with different standard deviations.

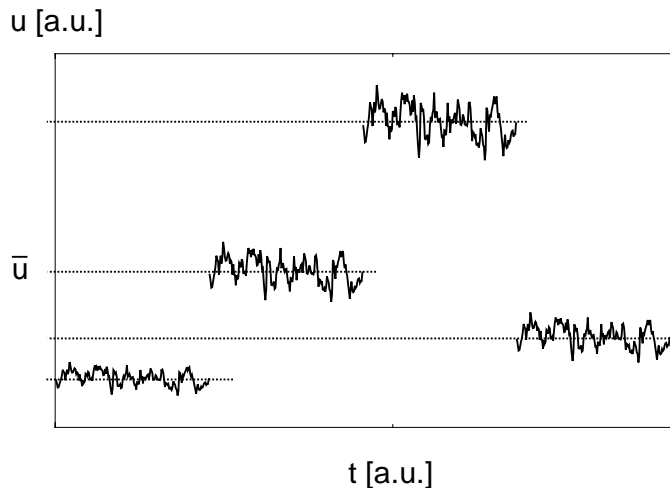


Figure 3.5: Illustration of different mean velocity intervals. Within these intervals statistics should be the same as for isotropic turbulence. The magnitude of variations (standard deviation) grows with mean velocity according to Eq. (3.24).

Thus we propose a model that describes the robust intermittent atmospheric PDFs as a superposition of those of isotropic turbulent subsets that are denoted with $p(u_\tau|\bar{u})$ and given by Eq. (3.11). Knowing the distribution of the mean velocity $h(\bar{u})$ the PDFs become:

$$p(u_\tau) = \int_0^\infty d\bar{u} h(\bar{u}) \cdot p(u_\tau|\bar{u}) \quad . \quad (3.18)$$

To find a suitable averaging time defining the mean value \bar{u} is a non-trivial problem due to the lack of a distinct mesoscale gap and is not the concern of the present paper (see e.g. [28]). As a first approximation we fix the averaging time

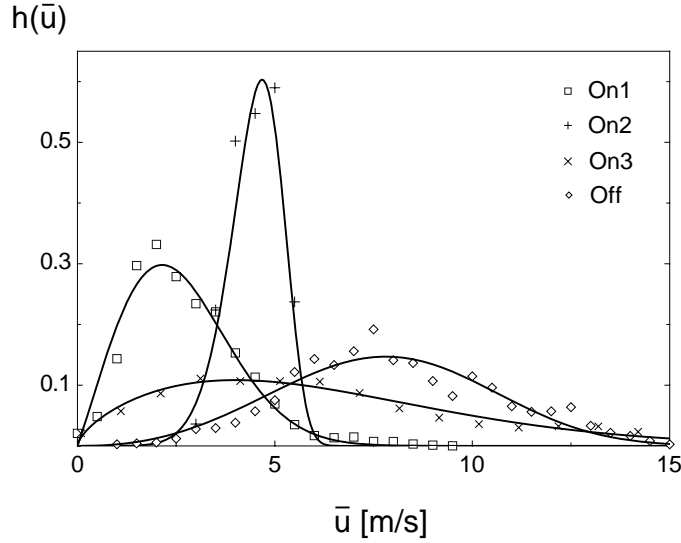


Figure 3.6: Symbols represent measured mean velocity distributions (averaged over 10 min) of the four atmospheric data sets *On1*, *On2*, *On3* and *Off*. Solid lines are fits according to Eq. (3.19). The parameters are: $k = 2.0, 7.8, 1.8, 3.3$ and $A = 2.9, 4.8, 7.1, 8.7$ for *On1*, *On2*, *On3* and *Off* respectively.

to be 10 minutes. In [4] it is shown that with this choice a partition into isotropic sequences is achieved. Furthermore we assume $h(\bar{u})$ to be a Weibull distribution

$$h(\bar{u}) = \frac{k}{A^k} \cdot \bar{u}^{k-1} \cdot \exp \left[- \left(\frac{\bar{u}}{A} \right)^k \right] , \quad (3.19)$$

that contains two parameters A and k . Both assumptions are well established in meteorology [1]. In Fig. 3.6 it is shown that the Weibull distribution $h(\bar{u})$ is a good representation of the measured distributions of mean velocities.

Inserting Eq. (3.19) and Eq. (3.11) into Eq. (3.18) the following expression for atmospheric PDFs is obtained:

$$p(u_\tau) = \frac{k}{2\pi A^k} \int_0^\infty d\bar{u} \int_0^\infty d\sigma \bar{u}^{k-1} \exp \left[- \left(\frac{\bar{u}}{A} \right)^k \right] \\ \times \frac{1}{\lambda\sigma^2} \exp \left[- \frac{u_\tau^2}{2\sigma^2} \right] \exp \left[- \frac{\ln^2(\sigma/\sigma_0)}{2\lambda^2} \right] . \quad (3.20)$$

Next we briefly discuss the meaning of the two parameters A and k . They play a similar role as σ_0 and λ^2 in the *Castaing distribution*. Parameter A is closely related to the expectation value ($\langle \bar{u} \rangle = A \cdot \Gamma(1 + k^{-1})$) of the mean velocity. Parameter k determines the shape of the distribution. Small values of k correspond to a broad distribution $h(\bar{u})$ so that many different mean velocities contribute

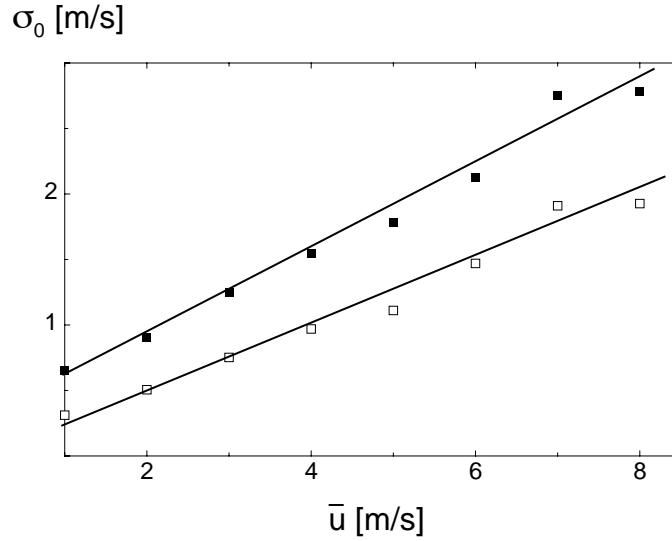


Figure 3.7: Standard deviation σ_0 as a function of \bar{u} for $\tau = 1s$ and $\tau = 50s$.

significantly to the integral in Eq. (3.20). Large k -values however prevent this contribution and $h(\bar{u})$ is closely centered around A . In the limit of very large k a delta distribution is obtained:

$$\lim_{k \rightarrow \infty} \left(\frac{k}{A^k} \bar{u}^{k-1} \exp \left[- \left(\frac{\bar{u}}{A} \right)^k \right] \right) = \delta(\bar{u} - A) \quad . \quad (3.21)$$

So for very large k -values Eq. (3.20) converges to Eq. (3.11) i.e. to isotropic turbulence. For additionally large τ and accordingly vanishing λ^2 one finally gets

$$\lim_{k \rightarrow \infty} \lim_{\tau \rightarrow \infty} p(u_\tau) = \frac{1}{\sigma_0 \sqrt{2\pi}} \exp \left[- \frac{u_\tau^2}{2\sigma_0^2} \right] \quad (3.22)$$

which is a pure Gaussian density with variance $\sigma_0^2(A)$. For small k -values the distributions remain intermittent even for large scales. Here intermittency is caused by the mixing of periods of different mean velocities.

To apply Eq. (3.20) to experimental data one has to know the parameters A , k , σ_0 and λ^2 . Parameters A and k can directly be estimated from data by fitting a Weibull distribution given in Eq. (3.19) to the measured distribution of \bar{u} . This is illustrated in Fig. 3.6 for all examined atmospheric data sets.

Next $\lambda^2 = \lambda^2(\tau, \bar{u})$ and $\sigma_0 = \sigma_0(\tau, \bar{u})$ have to be known. From isotropic turbulence it is well-established that the form parameter decreases monotonously in scale. Scaling of flatness according to Eq. (3.8) together with Eq. (3.13) directly leads to a logarithmic dependence of λ^2 on τ :

$$\lambda^2 = a_{\bar{u}} - b_{\bar{u}} \cdot \ln(\tau) \quad . \quad (3.23)$$

To confirm this in Fig. 3.4 the form parameter of the *Lab* data set is fitted with Eq. (3.23). For a deeper discussion on the scale dependence of λ^2 see [29].

The dependence of λ^2 on \bar{u} is small (e.g. [11] found a slower decay of λ^2 for increasing Reynolds numbers $Re \propto \bar{u}$). As a first approximation we will disregard it.

The parameter σ_0 – the most probable standard deviation – generally grows with scale and mean velocity. The scale dependence drops out automatically when considering normalized PDFs as it is done here. For the \bar{u} -dependence we assume a linear relation

$$s_0 = b_\tau \cdot \bar{u} \quad , \quad (3.24)$$

which is supported from the measured standard deviation σ_0 , shown in Fig. 3.7.

Thus, to apply Eq. (3.20) we need to calculate A and k from measured mean velocity distributions. Additionally we consider a logarithmic dependence of λ^2 on τ and a linear one for σ_0 on \bar{u} . Given that we are interested in a preferably simple reconstruction of PDFs by means of Eq. (3.20) we will disregard the more complex parameter relations here.

With these parameters atmospheric increment PDFs can be determined well from Eq. (3.20). As shown in Fig. 3.6 for *On1*, *On3* and *Off* rather small k -values of 2.0 1.8 and 3.3 are obtained indicating that resulting PDFs are heavy-tailed also for large scales. In Fig. 3.8 a) and 3.8 b) and Fig. 3.8 d) the corresponding PDFs as well as fits according to Eq. (3.20) are presented. The fits agree quite well with measured distributions. For all three data sets the tails show a similar decay for large scales and are close to a straight line which corresponds to an exponential decay due to the semi-logarithmic presentation.

In contrast to this behavior the PDFs of *On2* and the fits according to Eq. (3.20) – shown in Fig. 3.8 c) – approach a Gaussian distribution for large scales which is in accordance with the large k -value of 8.7 as it is found in Fig. 3.6. This large k -value mirrors the fact that *On2* was measured just over a short period of time (approximately 1 hour) with rather constant flow conditions. This means that as the flow becomes more and more stationary the superposition of different mean velocities becomes weaker and weaker. In the limit of a stationary velocity – as realized for *Lab* and approximately for *On2* – isotropic turbulence is recovered and large scale intermittency disappears.

Note, the intention of using Eq. (3.20) is not to get the best possible fits of the measured PDFs but to model PDFs at specific locations (with a specific mean velocity distribution) *a priori*. The measured PDFs could also be fitted by stretched exponential distributions [12] or by Eq. (3.11) as it is done in Fig. 3.3 b) for instance. These fits are based on *a posteriori* measurements however. Neither scaling models nor Eq. (3.11) are able to explain a flatness

larger than 3 and correspondingly intermittent PDFs for large scales outside of the inertial range as it is done by Eq. (3.20). This has interesting consequences for atmospheric velocities. For isotropic turbulence statistical properties of the flow can well be modelled. Thus knowing the composition of isotropic subsets it should be possible to model atmospheric velocity statistics as well.

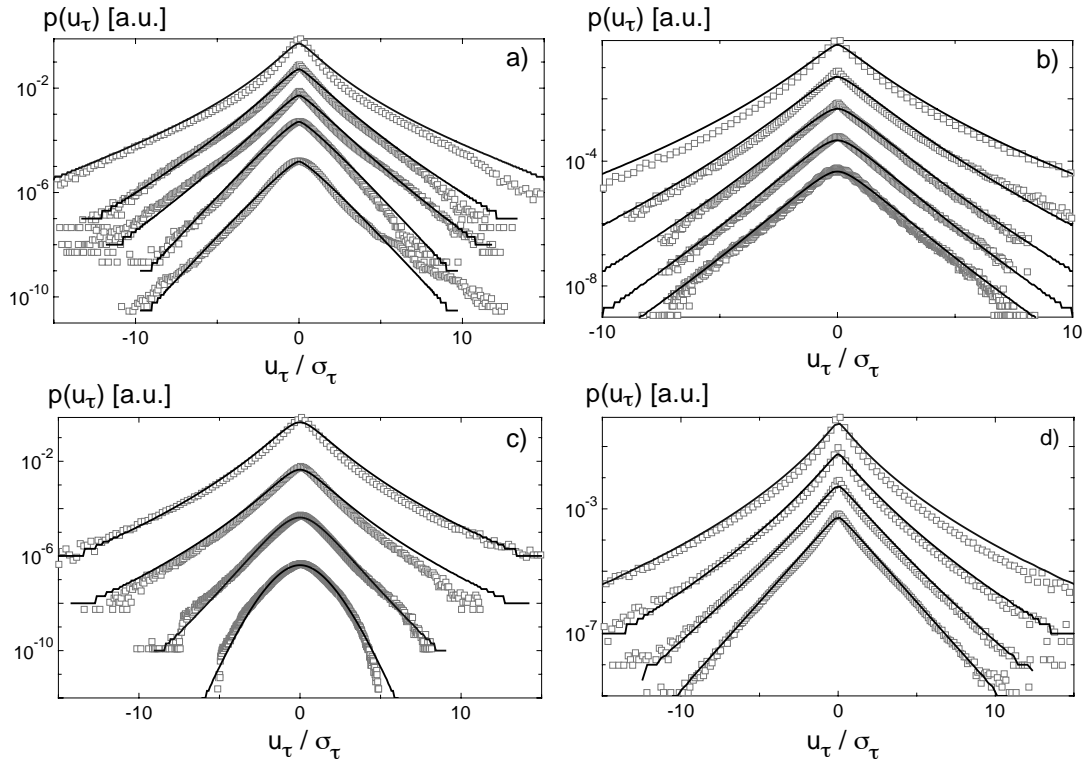


Figure 3.8: The symbols represent the normalized PDFs of the four atmospheric data sets in semi-logarithmic presentation. Solid lines correspond to a fit of distributions according to Eq. (3.20). All graphs are vertically shifted against each other for clarity of presentation. From top to bottom τ takes the following values: **a)** *Off*: 0.2s, 10s, 20s, 200s and 2000s. **b)** *On1*: 0.5s, 2.5s, 25s, 250s and 4000s. **c)** *On2*: 2ms, 20ms, 200ms and 2000ms. **d)** *On3*: 0.25s, 2.5s, 25s and 250s.

3.5 Conclusions

The presented analysis provides a good way to estimate and to explain robust and markedly intermittent PDFs of atmospheric increments. As desired the method recovers results of isotropic turbulence but is also able to take the large scale variations into account properly. A rigorous separation of time scales – which is very difficult – is not necessary for our model.

Standard analysis applied to isotropic turbulence cannot be transferred to long atmospheric time series unambiguously as it was shown by means of scaling behavior of structure functions and flatness. These methods are restricted to the inertial range where the change of shape can be more or less well reproduced and where at the large scale boundary of this range statistics become Gaussian.

It has been shown that the observed anomalous robust intermittency can be explained as a superposition of isotropic subsets in accordance with the concept of stable distributions. Intermittency on large scales is found to be the result of large scale mixing of isotropic turbulent subsets.

With our approach intermittent atmospheric PDFs can be approximated for any location as long as the mean velocity distribution is known. This is of importance for the construction of a wind turbine for instance. For constructing wind turbines only the turbulence intensity (relation between the average standard deviation and the mean velocity) is taken into account which is a very inadequate description. The loads are determined by increments and their occurrence statistics, therefore a model that reproduces the right increment distributions for every location should be preferred.

Acknowledgments

We acknowledge helpful discussions with *M. Siefert* and *B. Lange*. For data supply we further acknowledge *Risø National Laboratory* (offshore site funded by Energi E2/Seas), *Tauernwind Windkraftanlagen GmbH*, *Energiewerkstatt GmbH*, *J. Cleve* and *K. R. Sreenivasan*.

Bibliography

- [1] T. Burton, D. Sharpe, N. Jenkins, and E. Bossanyi. *Wind Energy Handbook*. John Wiley and Sons, 2001.
- [2] B. Lange, R. Barthelmie, and J. Hojstrup. Description of rodsand field measurement, 2001.
- [3] M. Ragwitz and H. Kantz. Indispensable finite time corrections for Fokker-Planck equations from time series data. *Phys. Rev. Lett.*, 87(25):254501, 2001.
- [4] F. Böttcher, C. Renner, H.P. Waldl, and J. Peinke. On the statistics of wind gusts. *Bound.-Layer Meteor.*, 108(1-2):163–173, 2003.
- [5] W. Bierbooms and P.-W. Cheng. Stochastic gust model for design calculations of wind turbines. *J. Wind. Eng. Ind. Aerodyn.*, 90(11):1237–1251, 2002.
- [6] I. van der Hoven. Power spectrum of horizontal wind speed in the frequency range from 0.0007 to 900 cycles per hour. *J. Meteorol.*, 14:160–164, 1957.
- [7] S. Lovejoy, D. Schertzer, and J. D. Stanway. Direct evidence of multifractal atmospheric cascades from planetary scales down to 1 km. *Phys. Rev. Lett.*, 86(22):5200–5203, 2001.
- [8] E. D. Eggleston and R. N. Clark. Cut-in note 1: Wind speed power spectrum analysis for bushland, Texas, USA. *Wind Engineering*, 24(1):49–52, 2000.
- [9] U. Frisch. Turbulence. The legacy of of A. N. Kolmogorov. *Cambridge University Press*, 1995.
- [10] J. Peinke, F. Böttcher, and St. Barth. Anomalous statistics in turbulence, financial markets and other complex systems. *Ann. Phys.*, 13(7-8):450–460, 2004.
- [11] B. Castaing, Y. Gagne, and E. J. Hopfinger. Velocity probability density functions of high Reynolds number turbulence. *Physica D*, 46(2):177–200, 1990.
- [12] D. Sornette. *Critical Phenomena in Natural Sciences*. Springer, 2000.
- [13] H. Hohlen and J. Liersch. Synchrone Messkampagnen von Wind- und Windkraftanlagen an Standort FH Ostfriesland, Emden. *DEWI Magazin*, 12:66–74, 1998.

- [14] G. Stolovitzky, P. Kailasnath, and K. R. Sreenivasan. Kolmogorov's refined similarity hypotheses. *Phys. Rev. Lett.*, 69(8):1178–1181, 1992.
- [15] H. Mellinghoff. Data evaluation of a wind measurement equipped with cup and sonic anemometers at Oberzeiring, Austria. *Report No.: DEWI-SO 0110-19*, 2001.
- [16] St. Lück. *Skalen aufgelöste Experimente und statistische Analysen von turbulenten Nachlaufströmungen*. PhD thesis, Carl-von-Ossietszky University of Oldenburg, 26111 Oldenburg, Germany, 2000.
- [17] C. Renner. *Markowanalysen stochastisch fluktuierender Zeitserien*. PhD thesis, Carl-von-Ossietszky University of Oldenburg, 26111 Oldenburg, Germany, 2002.
- [18] A. N. Kolmogorov. The local structure of turbulence in an incompressible viscous flow for very high Reynolds numbers. *Dokl. Acad. Nauk. SSSR*, 305:301–305, 1941.
- [19] A. N. Kolmogorov. A refinement of previous hypotheses concerning the local structure of turbulence in a viscous incompressible fluid at high Reynolds number. *J. Fluid Mech.*, 13:82–85, 1962.
- [20] A. Arneodo and C. Baudet et al. Structure functions in turbulence, in various flow configurations, at Reynoldsnumber between 30 and 5000, using extended self-similarity. *Europhys. Lett.*, 34(6):411–416, 1996.
- [21] Z.-S. She and E. Leveque. Universal scaling laws in fully developed turbulence universal scaling laws. *Phys. Rev. Lett.*, 72(3-4):336–339, 1994.
- [22] V. Yakhot. Probability density and scaling exponents of the moments of longitudinal velocity difference in strong turbulence. *Phys. Rev. E*, 57(2):1737–1751, 1998.
- [23] R. Benzi, S. Ciliberto, R. Tripicciono, C. Baudet, and S. Succi. Extended self-similarity in turbulent flows. *Phys. Rev. E*, 48(1):R29–R3, 1993.
- [24] C. Beck. Superstatistics in hydrodynamic turbulence. *Physica D*, 193:195–207, 2004.
- [25] C. Renner, J. Peinke, and R. Friedrich. Markov properties of small scale turbulence. *J. Fluid Mech.*, 433:383–409, 2001.
- [26] P. Lévy. *Théorie de l'addition des variables aléatoires*. Paris, Gauthier-Villars, 2e édition, 1954.

- [27] W. Paul and J. Baschnagel. *Stochastic Processes – From Physics to Finance*. Springer, 1999.
- [28] G. Trevino and E. L. Andreas. Averaging intervals for spectral analysis of nonstationary turbulence. *Bound.-Layer Meteor.*, 95(2):231–247, 2000.
- [29] B. Chabaud, A. Naert, J. Peinke, F. Chilla, B. Castaing, and B. Hébral. Transition toward developed turbulence. *Phys. Rev. Lett.*, 73(24):3227–3230, 1994.

Chapter 4

A generalized Method to distinguish between Dynamical and Measurement Noise in Complex Dynamical Systems

This article reports on a new method of analyzing measurement noise which is superimposed to a dynamical system. It is shown that external measurement noise and dynamical noise which is an intrinsic part of the dynamical process can be reconstructed from measured times series and that both can be distinguished well from each other. The distinction is based on the evaluation of the conditional moments that exhibit an increased offset with increasing measurement noise.

4.1 Introduction

A challenging problem for time series analysis of complex dynamical systems is given by the nonlinearity of the deterministic part as well as by the stochastic features. Such complex systems can often be described as a Langevin process which contains two coefficients – namely the drift and the diffusion coefficient – defining deterministic and stochastic influences.

Recently new progress in the non-parametric reconstruction of complex dynamics was achieved [1], [2], [3]. So it has been demonstrated that traffic flow dynamics [4], the chaotic dynamics of an electronic circuit [5], [6] or the human heart beat rhythm [7] can be reconstructed without need of any a priori models but just from measured time series, i.e. from estimated drift and diffusion coefficients. The evaluation of these coefficients generally encounters difficulties due to finite integration steps [8], [9], [10] and due to measurement noise which is usu-

ally superimposed to the dynamics supplementary. Both effects can lead to false estimations of the coefficients and can therefore prevent a proper reconstruction of the dynamics. In the following we focus on the influence of measurement noise presuming sufficiently small integration steps.

In [5], [6] and [11] a method has been introduced to separate measurement and dynamical noise and to estimate their magnitude by means of the second conditional moment. This moment exhibits an offset in the presence of measurement noise. The offset is directly related to the measurement noise amplitude given by its standard deviation σ . In addition to that the slope of the second conditional moment is equal to the diffusion coefficient (also called second Kramers-Moyal coefficient). The method is however restricted to low measurement noise. For large σ a systematic underestimation of measurement noise became evident while the slope could be still detected.

In this paper we propose a generalized method to estimate the amount of measurement noise for arbitrarily large values. In the first part of the paper the Langevin equation and the determination of drift and diffusion coefficients by means of conditional moments is summarized. Thereafter an example is given to point out the relevance of measurement noise for the reconstruction of complex dynamics. For a better understanding a univariate Ornstein-Uhlenbeck process is considered although the method is not restricted to it.

The crucial point of our work is that we can explain the measurement noise dependence of the first conditional moment – defining the drift coefficient (also called first Kramers-Moyal coefficient) – which was previously expected to be independent of the measurement noise. With this understanding we show that an improved parameter free reconstruction of the underlying Langevin process can be achieved.

4.2 The Langevin Equation

As basic system we consider a Langevin process that describes a stochastic process $X(t)$ in a variable t . For sufficiently small τ the evolution of an arbitrary realization $x(t)$ of such a process in iterative form is given by:

$$x(t + \tau) = x(t) + \tau D^{(1)}(x(t)) + \sqrt{D^{(2)}(x(t))} d\mathcal{W}(t) \quad . \quad (4.1)$$

Eq. (4.1) is an Itô stochastic differential equation which is connected to a Fokker-Planck equation that describes the process in probability space:

$$\frac{\partial}{\partial t} p(x, t) = \left[-\frac{\partial}{\partial x} D^{(1)}(x) + \frac{1}{2} \frac{\partial^2}{\partial x^2} D^{(2)}(x) \right] p(x, t) \quad . \quad (4.2)$$

The increments of a Wiener-process $d\mathcal{W}(t)$ can be considered as independent normally distributed random variables with $\langle d\mathcal{W}(t) \rangle = 0$ and $\langle (d\mathcal{W}(t))^2 \rangle = \tau$.

The Kramers-Moyal coefficients $D^{(1)}$ and $D^{(2)}$ are called drift and diffusion coefficients. They can directly be derived from the conditional moments $M^{(n)}$ (with $n = 1, 2$) defined as:

$$M^{(n)}(x, \tau) = \langle [x(t + \tau) - x(t)]^n \rangle |_{x(t)=x} . \quad (4.3)$$

The rhs. of Eq. (4.3) denotes an average under the condition that $x(t)$ is equal to x . Conditional moments and drift and diffusion coefficients are related to each other according to:

$$\begin{aligned} M^{(1)}(x, \tau) &= \tau D^{(1)} + \frac{\tau^2}{2} D^{(1)} \partial_x D^{(1)} + \frac{\tau^2}{4} D^{(2)} \partial_{xx}^2 D^{(1)} + \mathcal{O}(\tau^2) \\ M^{(2)}(x, \tau) &= \tau D^{(2)} + \tau^2 (D^{(1)})^2 + \tau^2 D^{(2)} \partial_x D^{(1)} + (\dots) + \mathcal{O}(\tau^3) . \end{aligned} \quad (4.4)$$

This expression is obtained from expanding Eq. (4.1) into an *Itô-Taylor series* (for a detailed discussion see e.g. [12], [13]). As indicated by the brackets on the rhs. of Eq. (4.4) further terms quadratic in τ arise containing derivations of $D^{(2)}$ (compare [9], [10]). For the hereafter considered Ornstein-Uhlenbeck process – exhibiting a linear drift and constant diffusion coefficient – they do not contribute to Eq. (4.4). The terms quadratic in τ and in particular all higher order terms are significant only for large τ and large coefficients $D^{(n)}$. For sufficiently small τ or $D^{(n)}$ the Euler approximation which is

$$\begin{aligned} M^{(1)}(x, \tau) &\approx \tau D^{(1)}(x) \\ M^{(2)}(x, \tau) &\approx \tau D^{(2)}(x) + \tau^2 (D^{(1)}(x))^2 \end{aligned} \quad (4.5)$$

should be sufficient¹. From the conditional moments drift and diffusion coefficients can be obtained from Eq. (4.4) as well as from Eq. (4.5) by:

$$D^{(n)}(x) = \lim_{\tau \rightarrow 0} \frac{1}{\tau} M^{(n)}(x, \tau) . \quad (4.6)$$

The drift coefficient $D^{(1)}$ describes the deterministic part of the Langevin process while $D^{(2)}$ can be considered as the amplitude of the stochastic, noisy part. Due to the fact that this random contribution directly influences the dynamics it is also referred to as *dynamical noise*. If the diffusion coefficient depends on x the stochastic part $\sqrt{D^{(2)}} d\mathcal{W}(t)$ is called multiplicative otherwise additive noise.

In addition to dynamical noise external *measurement noise* $\sigma \zeta(t)$, with $\langle \zeta(t) \rangle = 0$ and $\langle \zeta(t)^2 \rangle = 1$, might be superimposed to a Langevin process. This kind of noise is not influencing the dynamics but is added to it posterior. Therefore its amplitude σ is independent of the process and independent of

¹Note that the demand for small coefficients might be seen in analogy to the demand of small time steps. In both cases $x(t + \tau) - x(t)$ is small compared to the total range of values.

x . External noise might be present due to diverse reasons like limitations in measuring devices, the signal processing procedure and so forth. For a proper reconstruction of an underlying Langevin process the amount of measurement noise should be known as exact as possible which is demonstrated in the following example.

Let us consider a Langevin process with multiplicative noise. The drift coefficient is defined as $D^{(1)}(x) = ax$ and the diffusion coefficient as $D^{(2)}(x) = b + cx^2$ with the parameters $a = -0.002$, $b = 0.0001$ and $c = 0.003$. For b -values small compared to c the contribution of multiplicative noise is dominating the dynamics. In this case the probability density function $p(x)$ of the variable x is found to be markedly intermittent. Superimposing measurement noise with large σ ($\sigma = 0.5$) to the time series the intermittent character of the distribution vanishes as can be seen in Fig. 4.1 where the probability density function of the increments – defined as $x_\Delta := x(t + \Delta) - x(t)$ – are presented. Increment statistics are intensively studied in the context of the analysis of turbulent flows or financial data (e.g. [11], [14]).

For time series with superimposed external noise it might thus become very difficult to grasp the essential features of the real underlying dynamics.

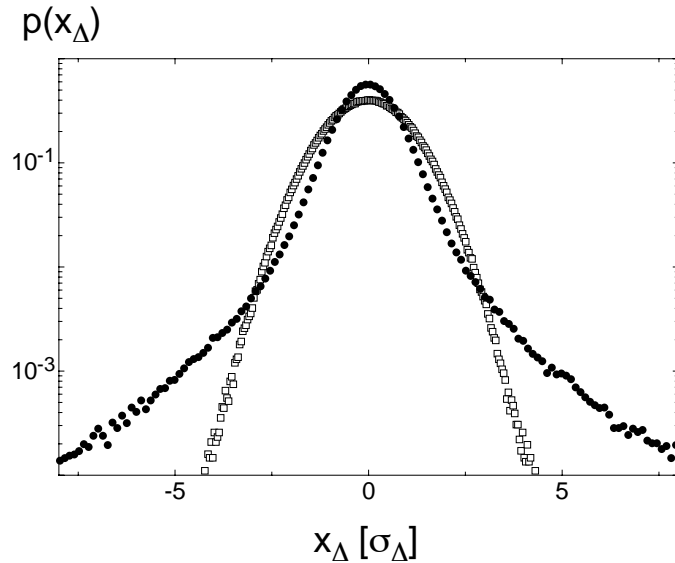


Figure 4.1: Filled symbols (\bullet) represent the increment distribution of a process with multiplicative noise, the open symbols (\square) that of the same process but with superimposed measurement noise which is very close to a Gaussian one. Both distributions are plotted in semi-logarithmic presentation and are normalized with the corresponding standard deviation $\sigma_\Delta = \sqrt{\langle (x_\Delta)^2 \rangle}$.

4.3 Measurement Noise

To discuss the effect of adding measurement noise to a Langevin process we first calculate the conditional moments for (i) a pure noise signal $\sigma\zeta(t)$ and for (ii) a pure Langevin process $x(t)$. After that (iii) a Langevin process plus measurement noise $y(t) = x(t) + \sigma\zeta(t)$ is addressed. Obviously (i) and (ii) are limiting cases of the third one for very large and very small measurement noise amplitudes.

(i): For pure noise the conditional moments do not depend on τ and read:

$$\begin{aligned} M^{(1)}(\mathbf{x}, \tau) &= \langle \sigma\zeta(t + \tau) - \sigma\zeta(t) \rangle |_{\sigma\zeta(t)=\mathbf{x}} \\ &= -\mathbf{x} \\ M^{(2)}(\mathbf{x}, \tau) &= \langle (\sigma\zeta(t + \tau) - \sigma\zeta(t))^2 \rangle |_{\sigma\zeta(t)=\mathbf{x}} \\ &= \sigma^2 + \mathbf{x}^2 \quad . \end{aligned} \quad (4.7)$$

Note that in the following bold letters – like \mathbf{x} in Eq. (4.7) – are used to stress the phase space value on which the condition is performed. It should not be confused with a vector notation. The non-dependence on τ which is characteristic of noise causes a divergence of the corresponding coefficients $D^{(1)}$ and $D^{(2)}$ in the limit of vanishing τ as can be seen from inserting Eq. (4.7) into Eq. (4.6).

(ii): Here both coefficients are well defined which can readily be checked inserting Eq. (4.1) in Eq. (4.3). Exemplary for the first moment one obtains:

$$\begin{aligned} M^{(1)}(\mathbf{x}, \tau) &= \langle x(t + \tau) - x(t) \rangle |_{x(t)=\mathbf{x}} \\ &= \left\langle \tau D^{(1)}(\mathbf{x}) - \sqrt{D^{(2)}(\mathbf{x})} d\mathcal{W}(t) \right\rangle |_{x(t)=\mathbf{x}} = \tau D^{(1)}(\mathbf{x}) \quad . \end{aligned} \quad (4.8)$$

(iii): In [5] it has been argued that for small σ -values the drift coefficient is the same as for case (ii) whereas the diffusion coefficient has to be corrected. The moments were found to be:

$$\begin{aligned} M^{(1)}(\mathbf{y}, \tau) &= \langle x(t + \tau) - x(t) + \sigma\zeta(t + \tau) - \sigma\zeta(t) \rangle |_{y(t)=\mathbf{y}=x(t)+\sigma\zeta(t)} \\ &= \tau D^{(1)}(x) \\ M^{(2)}(\mathbf{y}, \tau) &= \langle (x(t + \tau) - x(t) + \sigma\zeta(t + \tau) - \sigma\zeta(t))^2 \rangle |_{y(t)=\mathbf{y}=x(t)+\sigma\zeta(t)} \\ &= \tau D^{(2)}(x) + 2\sigma^2 \quad . \end{aligned} \quad (4.9)$$

This means that due to the offset $2\sigma^2$ the diffusion coefficient diverges as τ goes to zero. The symbol \mathbf{y} reflects the fact that it is not the dynamical state x but the measured value $\mathbf{y} = x(t) + \sigma\zeta(t)$ on which the condition is performed. As it has already been mentioned in [5] the estimation of moments is restricted to rather small amplitudes of measurement noise (amplitudes no larger than $\sigma \approx 0.04\sqrt{D^{(2)}}$ were considered.) so that y and x are close to each other.

To grasp the influence of large measurement noise amplitudes an Ornstein-Uhlenbeck process with $D^{(1)}(x) = -0.002x$ and $D^{(2)}(x) = 0.002$ and unit time

steps $\tau = 1$ is generated. Subsequently measurement noise with different amplitudes was superimposed to the resulting time series² and the conditional moments were estimated according to Eq. (4.3).

In Fig. 4.2 a) the first and the second conditional moments are plotted for different measurement noise amplitudes. Both moments show an increased offset with increasing σ . This offset causes a divergent behavior of $\frac{1}{\tau}M^{(n)}(\mathbf{y}, \tau)$ as shown in Fig. 4.2 b). Therefore the Kramers-Moyal coefficients estimated by means of Eq. (4.6) would become larger and larger with decreasing τ . It should be noted that for $\sigma = 0.2$ and $\tau = 1$ the estimate of the drift coefficient using Eq. (4.6) is already 11 times larger than the real $D^{(1)}$. Compared to that $D^{(1)}$ and $D^{(2)}$ can be estimated well when fitting the slope of $M^{(n)}(\mathbf{y}, \tau)$. In this case the error is smaller than 7%. The fitted slopes are indicated by the straight and dashed lines in Fig. 4.2.

From these findings we conclude that

$$M^{(n)}(\mathbf{y}, \tau) = \tau D^{(n)}(x) + \gamma_n(\mathbf{y}, \sigma) \quad . \quad (4.10)$$

should be a good ansatz for the first and the second conditional moment in the case of strong measurement noise. Next we show how to evaluate $\gamma_n(\mathbf{y}, \sigma)$.

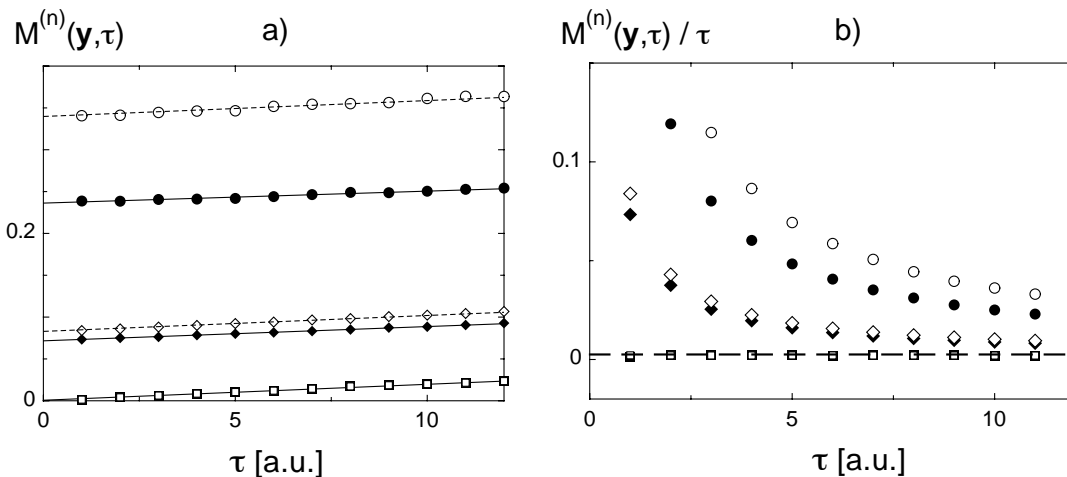


Figure 4.2: Conditional moments for different amplitudes of measurement noise. These are $\sigma = 0.0$ (squares), $\sigma = 0.2$ (diamonds) and $\sigma = 0.4$ (circles) which corresponds to 0%, 450% and 900% of the dynamical noise amplitude $\sqrt{D^{(2)}} \approx 0.045$.

a) $M^{(n)}(\mathbf{y}, \tau)$ at $\mathbf{y} = -1$: Filled symbols correspond to $M^{(1)}$, the open ones to $M^{(2)}$. The straight lines are linear fits which determine $D^{(1)}$ and $D^{(2)}$.

b) $\frac{1}{\tau}M^{(n)}(\mathbf{y}, \tau)$ at $\mathbf{y} = -1$ for the same data as in a). The real values of $D^{(n)}$ are indicated by the dashed line.

²The random numbers were generated by means of a Box-Muller algorithm.

4.4 Offset of the Conditional Moments

To explain the offset γ_1 we start with the definition of $M^{(1)}$ for the experimentally accessible values $y(t)$:

$$M^{(1)}(\mathbf{y}, \sigma) = \langle y(t + \tau) - y(t) \rangle |_{y(t)=\mathbf{y}=x(t)+\sigma\zeta(t)} \quad . \quad (4.11)$$

These moments can be decomposed into two parts. The one part contains all those cases where \mathbf{y} is very close to x and thus $\sigma \approx 0$. The second part covers all other states where \mathbf{y} differs significantly from x , i.e. $\sigma \gg 0$. We thus obtain the following expression:

$$\begin{aligned} M^{(1)}(\mathbf{y}, \tau) &= \langle y(t + \tau) - y(t) \rangle |_{\mathbf{y}=x} + \langle y(t + \tau) - y(t) \rangle |_{\sigma\zeta(t)=\mathbf{y}-x} \\ &= \langle x(t + \tau) - x(t) \rangle |_{\mathbf{y}=x} + \langle x(t + \tau) - x(t) \rangle |_{\sigma\zeta(t)=\mathbf{y}-x} \\ &\quad + \langle \sigma\zeta(t + \tau) - \sigma\zeta(t) \rangle |_{\mathbf{y}=x} + \langle \sigma\zeta(t + \tau) - \sigma\zeta(t) \rangle |_{\sigma\zeta(t)=\mathbf{y}-x} \\ &= \langle x(t + \tau) - x(t) \rangle |_{\mathbf{y}=x} + \langle \sigma\zeta(t) \rangle |_{\sigma\zeta(t)=x-\mathbf{y}} \\ &= M^{(1)}(x = \mathbf{y}, \tau) + \langle x - \mathbf{y} \rangle \\ &= \tau D^{(1)}(x = \mathbf{y}, \tau) + \gamma_1(\sigma, \mathbf{y}) \quad . \end{aligned} \quad (4.12)$$

This means that the additional offset comes from the expectation value of the difference between \mathbf{y} and $x(t)$.

For an underlying linear drift it might be expected that smaller and larger values compensate each other because the measurement noise is distributed symmetrically around the process $x(t)$. In this case $\langle x(t) - \mathbf{y} \rangle$ is expected to be zero and Eq. (4.12) would reduce to Eq. (4.9).

As illustrated in Fig. 4.3 the value \mathbf{y} can be reached from all of the $x(t)$ with a probability decaying symmetrically with respect to the distance between $x(t)$ and \mathbf{y} . The probability to find a value $x(t)$ however decreases with increasing distance to its mean value $\langle x(t) \rangle = 0$. This means that for positive \mathbf{y} (or more generally for $\mathbf{y} > \langle x(t) \rangle$), more $x(t)$ -values smaller than \mathbf{y} contribute to the estimation of $M^{(1)}$ than $x(t)$ -values larger than \mathbf{y} . For negative \mathbf{y} the situation is reversed. This effect is illustrated schematically in Fig. 4.3 where the darker shade denotes an increased probability for $x(t)$ to be below \mathbf{y} .

On the basis of these considerations the expectation value $\langle x(t) - \mathbf{y} \rangle$ can be calculated according to:

$$\gamma_1 = \langle x(t) - \mathbf{y} \rangle = \int_{-\infty}^{\infty} dx (x - \mathbf{y}) \cdot p(x) \cdot f(x - \mathbf{y}) \quad . \quad (4.13)$$

For the here-considered Ornstein-Uhlenbeck process $p(x)$ is known to be a Gaussian distribution with variance $s^2 = D^{(2)}/(2D^{(1)})$. The distribution $f(x - \mathbf{y})$ of

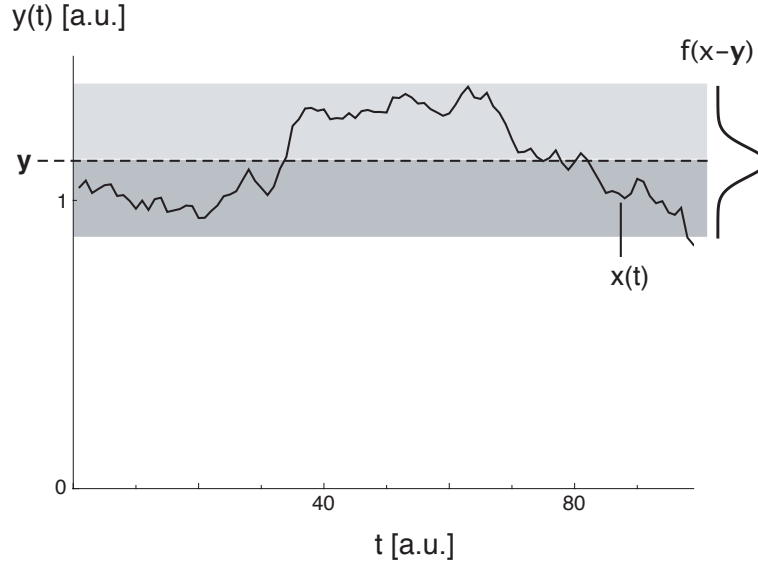


Figure 4.3: The solid line represents a Langevin process $x(t)$, the dashed line denotes the value \mathbf{y} on which is conditioned. The gray area symbolizes those states x that can contribute to \mathbf{y} due to the superimposed measurement noise. The probability of such a contribution decreases according to a Gaussian distribution $f(x - \mathbf{y})$ that is schematically drawn in at the right side of the time series. The darker shade of the states x smaller than \mathbf{y} mirrors the fact that these are more likely to occur than those larger than \mathbf{y} .

the superimposed measurement noise is also Gaussian with variance σ^2 . Thus γ_1 can be given explicitly:

$$\begin{aligned} \gamma_1(\mathbf{y}, \sigma) &= \frac{1}{N} \int_{-\infty}^{\infty} dx (x - \mathbf{y}) \exp \left[-\frac{x^2}{2s^2} - \frac{(x - \mathbf{y})^2}{2\sigma^2} \right] \\ &= -\frac{\sigma^2}{\sigma^2 + s^2} \cdot \mathbf{y} \quad . \end{aligned} \quad (4.14)$$

N is the normalization constant and is given by the convolution of both distributions $p(x) * f(x - \mathbf{y})$.

To check whether Eq. (4.14) describes the offsets of the first conditional moment correctly we calculate them from numerical data of the above mentioned Ornstein-Uhlenbeck process for different combinations of σ and \mathbf{y} . In Fig. 4.4 a) $\gamma_1(\mathbf{y}, \sigma)$ has been plotted as a function of \mathbf{y} for two different σ -values. In Fig. 4.4 b) \mathbf{y} is constant and σ varies. In both cases the measured offsets correspond well to the calculated ones according to Eq. (4.14). This correspondence refers to both limits, $\lim_{\sigma \rightarrow \infty} \gamma_1(\mathbf{y}, \sigma) = -\mathbf{y}$ and $\lim_{\sigma \rightarrow 0} \gamma_1(\mathbf{y}, \sigma) = 0$, as well as to the intermediate range of measurement noise amplitudes.

Thus we summarize, for the first conditional moment of an Ornstein-Uhlenbeck process the observed offset γ_1 turns out to be identical to the

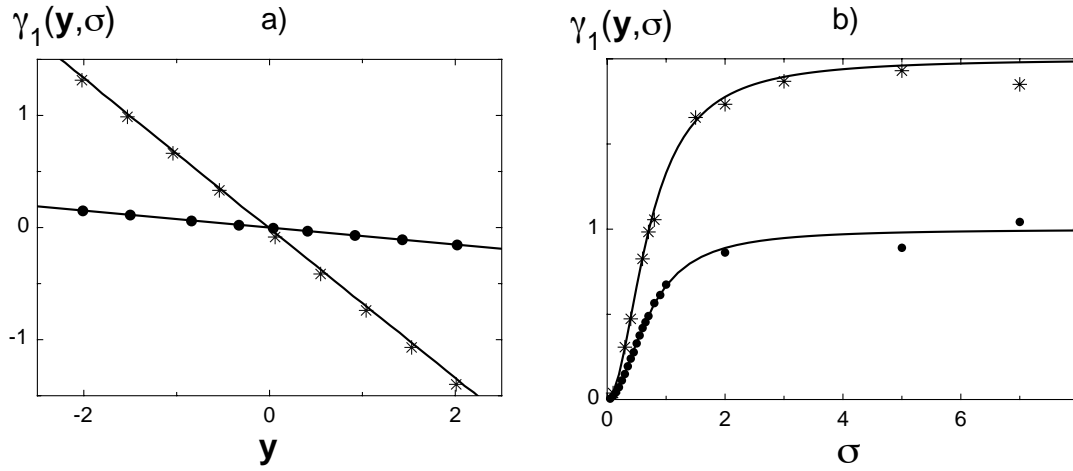


Figure 4.4: **a)** The symbols represent the measured offset as a function of \mathbf{y} for $\sigma = 0.2$ (\bullet) and $\sigma = 1$ ($*$) respectively. The straight lines show the expected offsets $\gamma_1(\mathbf{y}, \sigma)$ according to Eq. (4.14).

b) The symbols represent the measured offset as a function of σ at $\mathbf{y} = -1$ (\bullet) and at $\mathbf{y} = -2$ ($*$). The solid lines correspond to the expected offsets $\gamma_1(\mathbf{y}, \sigma)$ according to Eq. (4.14).

expectation value $\langle x(t) - \mathbf{y} \rangle$.

Similar to the discussion of the first moment $M^{(1)}$, the offset of the second conditional moment is affected by the condition on \mathbf{y} so that a deviation from $2\sigma^2$ – as suggested by Eq. (4.9) – should be observed. In analogy to the first conditional moment the second one exhibits an additional offset stemming from the expected difference between x and \mathbf{y} :

$$\begin{aligned} \gamma_2(\mathbf{y}, \sigma) &= \langle (x(t) - \mathbf{y})^2 \rangle = \frac{1}{N} \int_{-\infty}^{\infty} dx (x - \mathbf{y})^2 \exp \left[-\frac{x^2}{2s^2} - \frac{(x - \mathbf{y})^2}{2\sigma^2} \right] \\ &= \frac{\sigma^2 s^4 + \sigma^4 s^2}{(\sigma^2 + s^2)^2} + \frac{\sigma^4}{(\sigma^2 + s^2)^2} \cdot \mathbf{y}^2 . \end{aligned} \quad (4.15)$$

N is given by $p(x) * f(x - \mathbf{y})$. The derivation of the integrals γ_1 and γ_2 is given in Appendix C. The offset $\tilde{\gamma}_2(\mathbf{y}, \sigma)$ – obtained from the numerical data – is found to be the sum of Eq. (4.15) and the variance of the measurement noise σ^2 as it is presented in Fig. 4.5 a) and b):

$$\tilde{\gamma}_2(\mathbf{y}, \sigma) = \gamma_2(\mathbf{y}, \sigma) + \sigma^2 . \quad (4.16)$$

In Fig. 4.5 a) $\tilde{\gamma}_2(\mathbf{y}, \sigma)$ has been plotted as a function of \mathbf{y} for two different σ -values. In Fig. 4.5 b) $\gamma_2(\mathbf{y}, \sigma)$ as a function of σ for two different \mathbf{y} -values is presented. In both cases the offsets correspond well to the calculated ones

according to Eq. (4.15) and Eq. (4.16). For large measurement noise amplitudes $\gamma_2(\mathbf{y}, \sigma)$ approaches $\mathbf{y}^2 + s^2$ while for small ones it approaches σ^2 as it can also be seen in Fig. 4.5 a) and b).

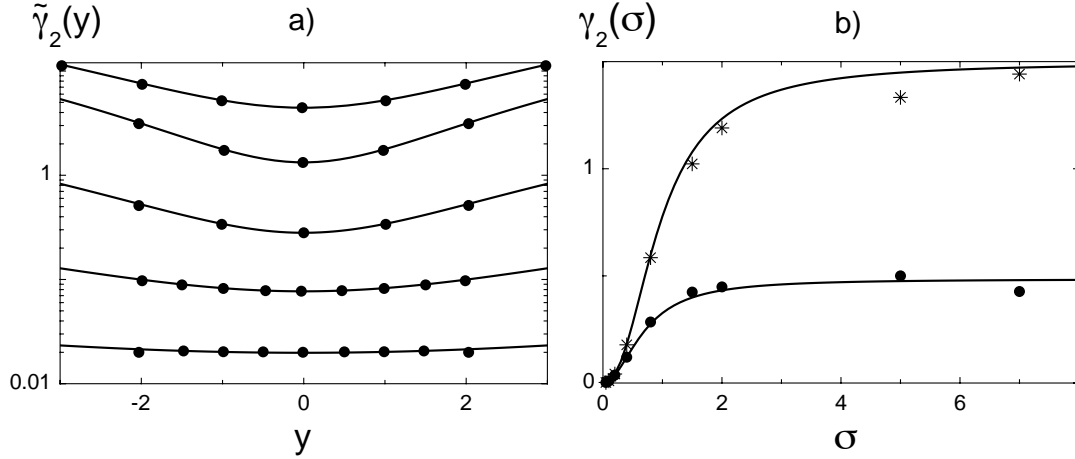


Figure 4.5: **a)** The symbols (\bullet) represent the measured offset $\gamma_2(\mathbf{y}, \sigma)$ as a function of y for (from bottom to top) the σ -values 0.1, 0.2, 0.4, 1.0 and 2.0 in a semi-logarithmic presentation. The solid lines show the expected offsets according to Eq. (4.16).

b) The symbols represent the measured offset $\gamma_2(\mathbf{y}, \sigma) - \sigma^2$ as a function of σ at $\mathbf{y} = 0$ (\bullet) and at $\mathbf{y} = -1$ ($*$). The solid lines correspond to the expected offsets according to Eq. (4.15).

For an Ornstein-Uhlenbeck process Eq. (4.14) and (4.16) allow to calculate both, the standard deviation of the underlying process s and that of the measurement noise σ because for fixed \mathbf{y} they are the only two variables entering the two equations. This means in particular that even if the dynamics is completely covered by external measurement noise the standard deviation $s = \sqrt{D^{(2)}/(2D^{(1)})}$ can still be estimated measuring the offset of the first and second conditional moment. Here one should note that the required resolution as well as the number of data points will increase with σ .

So far the offsets have only been calculated for an Ornstein-Uhlenbeck process. For more complicated situations such as processes with multiplicative noise for instance $p(x)$ is not necessarily Gaussian distributed. Nevertheless the expected difference $\gamma_n = \langle (x - \mathbf{y})^n \rangle$ (with $n = 1, 2$) can be calculated numerically if the stochastic variable x obeys the stationary solution [15]:

$$p(x) = \frac{\mathcal{N}}{D^{(2)}(x)} \cdot \exp \left[2 \int_{-\infty}^x \frac{D^{(1)}(x')}{D^{(2)}(x')} dx' \right]. \quad (4.17)$$

\mathcal{N} denotes a proper normalization constant. Additionally to $\langle (x - \mathbf{y})^n \rangle$ the offset will then be caused by the non-linearity of the coefficients.

For our understanding so far, to grasp the influence of measurement noise for more complicated processes, one should estimate drift and diffusion coefficient by means of the slope of the moments. For two exemplary processes – defined by a) $D^{(1)}(x) = -0.001x^3$, $D^{(2)}(x) = 0.001$ and b) $D^{(1)}(x) = -0.002x$, $D^{(2)}(x) = 0.0005 + 0.001x^2$ we have checked the estimation of coefficients. For $\sigma = 0.2$ and even larger the coefficients can be reconstructed well by our proposition to analyze the slopes of the conditional moments. Knowing $D^{(1)}$ and $D^{(2)}$ the distribution $p(x)$ can be calculated according to Eq.(4.17). Under the assumption of Gaussian distributed measurement noise and using Eq. (4.14) and (4.15) the offsets γ_1 and γ_2 can at last be obtained.

4.5 Summary

The determination of the conditional moments provides an elegant way to estimate drift and diffusion coefficients of an underlying Langevin-process by means of the slope of the moments. In addition to that the strength of external measurement noise can be evaluated by means of the offsets of the conditional moments. The (increasing) offsets as a function on σ can be used to quantify the transition from a pure stochastic process ($\sigma = 0$) to a pure noise signal ($\sigma \gg 1$).

Compared to former works we were able to generalize the behavior of conditional moments to the case of large measurement noise amplitudes. In addition to that we could for the first time explain the offset of the first conditional moment. For an Ornstein-Uhlenbeck process the offsets of the first and the second moment are analytically explained.

We want to stress that the evaluation of external noise by estimating the offset of the conditional moments is not restricted to small noise amplitudes but should be possible for any noise level. Furthermore it should be possible to extend the method to more general processes than the analyzed Ornstein-Uhlenbeck process if the process variable obeys the stationary solution specified by Eq. (4.17). In this case more challenging methods of parameter optimizations are likely to be necessary.

Bibliography

- [1] S. Siegert, R. Friedrich, and J. Peinke. Analysis of data sets of stochastic systems. *Phys. Lett. A*, 243:275–280, 1998.
- [2] R. Friedrich, S. Siegert, J. Peinke, St. Lueck, M. Siefert, M. Lindemann, J. Raethjen, G. Deuschl, and G. Pfister. Extracting model equations from experimental data. *Phys. Lett. A*, 271:217–222, 2000.
- [3] J. Gradisek, S. Siegert, R. Friedrich, and I. Grabec. Analysis of time series from stochastic processes. *Phys. Rev. E*, 62:3146–3155, 2000.
- [4] S. Kriso, J. Peinke, R. Friedrich, and P. Wagner. Reconstruction of dynamical equations for traffic flow. *Phys. Lett. A*, 299:287–291, 2002.
- [5] M. Siefert, A. Kittel, R. Friedrich, and J. Peinke. On a quantitative method to analyze dynamical and measurement noise. *Europhys. Lett.*, 61:466–472, 2003.
- [6] M. Siefert and J. Peinke. Reconstruction of the deterministic dynamics of stochastic systems. *Int. J. Bifurcation and Chaos*, 14(6):2005–2010, 2004.
- [7] T. Kuusela. Stochastic heart-rate model can reveal pathologic cardiac dynamics. *Phys. Rev. E*, 69:031916, 2004.
- [8] M. Ragwitz and H. Kantz. Indispensable finite time corrections for Fokker-Planck equations from time series data. *Phys. Rev. Lett.*, 87(25):254501, 2001.
- [9] R. Friedrich, C. Renner, M. Siefert, and J. Peinke. Comment on "Indispensable finite time corrections for Fokker-Planck equations from time series data". *Phys. Rev. Lett.*, 89:149401, 2002.
- [10] P. Sura and J. Barsugli. A note on estimating drift and diffusion parameters from timeseries. *Phys. Lett. A*, 305(5):304–311, 2002.
- [11] C. Renner, J. Peinke, and R. Friedrich. Evidence of Markov properties of high frequency exchange rate data. *Physica A*, 298:499–520, 2001.
- [12] J. Hohnerkamp. *Stochastische Dynamische Systeme*. VCH, Weinheim, 1990.
- [13] P. E. Kloeden and E. Platen. *Numerical Solution of Stochastic Differential Equations*. Springer, 1999.

- [14] C. Renner, J. Peinke, R. Friedrich, O. Chanal, and B. Chabaud. Universality of small scale turbulence. *Phys. Rev. Lett.*, 89:124502, 2002.
- [15] C. W. Gardiner. *Handbook of Stochastic Methods*. Springer Verlag, 1985.

Appendix A

Gust Definitions

Besides the **Extreme operating gusts (EOG)** the *IEC 61400-1* norm contains four other gust definitions.

- **Extreme direction changes (EDC)**: The angle is given by

$$\Theta_{eN} = \pm\beta \cdot \arctan\left(\frac{\sigma}{u_z(1 + (D/10\Lambda))}\right),$$

while the shape is determined by:

$$\Theta_N(t) = \begin{cases} 0 & , t < 0 \\ \frac{1}{2}\Theta_{eN} (1 - \cos(\frac{\pi t}{T})) & , 0 \leq t \leq T \\ \Theta_{eN} & , t > T \end{cases} . \quad (\text{A.1})$$

For the duration of an extreme direction change $T = 6s$ is assumed.

- **Extreme coherent gusts (ECG)**: The magnitude is given by:

$$u_{cg} = 15ms^{-1}.$$

The shape is defined as follows:

$$u_z(t) = \begin{cases} u_z & , t < 0 \\ u_z + \frac{1}{2}u_{cg}(1 - \cos(\frac{\pi t}{T})) & , 0 \leq t \leq T \\ u_z + u_{cg} & , t > T \end{cases} \quad (\text{A.2})$$

For the duration of an extreme coherent gust $T = 10s$ is assumed. u_z is the wind speed at height z before the gust occurs.

- **Extreme coherent gusts with direction change (ECD)**: Here the wind speed rise of an extreme coherent gust is assumed to occur simultaneously with a direction change specified by:

$$\Theta_{cg}(u_z) = \begin{cases} 180^\circ & , u_z < 4ms^{-1} \\ 720^\circ ms^{-1}/u_z & , 4ms^{-1} \leq u_z \leq u_{ref} \end{cases}$$

u_{ref} is a reference velocity also specified in IEC 61400-1. The shape is defined as follows:

$$\Theta(t) = \begin{cases} 0^\circ & , t < 0 \\ \pm \frac{1}{2} \Theta_{cg} (1 - \cos(\frac{\pi t}{T})) & , 0 \leq t \leq T \\ \pm \Theta_{cg} & , t > T \end{cases} . \quad (\text{A.3})$$

The duration of the extreme coherent gust with direction change is assumed to be $T = 10s$.

- **Extreme wind shears (EWS):** For transient vertical shears they are defined as:

$$u_z(t) = \begin{cases} u_z + \frac{(z-z_0)}{D} \left(\frac{5}{2} + \frac{\beta\sigma}{5} \left(\frac{D}{\Lambda} \right)^{\frac{1}{4}} \right) (1 - \cos(\frac{2\pi}{T}t)) & , 0 \leq t \leq T \\ u_z & , else \end{cases} .$$

For transient horizontal shears:

$$u_z(t) = \begin{cases} u_z + \frac{y}{D} \left(\frac{5}{2} + \frac{\beta\sigma}{5} \left(\frac{D}{\Lambda} \right)^{\frac{1}{4}} \right) (1 - \cos(\frac{2\pi}{T}t)) & , 0 \leq t \leq T \\ u_z & , else \end{cases} . (\text{A.4})$$

For an extreme wind shear the recurrence time is $N = 50a$ and $\beta = 6.4$. The duration is $T = 12s$.

In all cases D denotes the diameter of the turbine and Λ is a reference scale, σ is the standard deviation and u_z is the velocity at height z .

Appendix B

Superstatistics

Generally the marginal distribution $p(u_\tau)$ can be obtained from the superposition (hence the name 'superstatistics'.) of Gaussian distributions with variance $\sigma^2 \propto \beta^{-1}$ and the distribution $f(\beta)$. The standard model in turbulence is a lognormal distribution of β . Beck showed that $f(\beta)$ is not necessarily a lognormal but can also be another distribution. For a χ^2 -distribution he derived the following marginal distribution:

$$\begin{aligned}
 p(u_\tau) &= \int_0^\infty d\beta p(u_\tau|\beta) \cdot f(\beta) \\
 &= \int_0^\infty d\beta \sqrt{\beta/2\pi} \exp\left[-\frac{\beta u_\tau^2}{2}\right] \cdot \frac{1}{\Gamma(n/2)} \left(\frac{n}{2\beta_0}\right)^{n/2} \beta^{\frac{n}{2}-1} \exp\left[-\frac{n\beta}{2\beta_0}\right] \\
 &= \frac{1}{\sqrt{2\pi}\Gamma(n/2)} \left(\frac{n}{2\beta_0}\right)^{n/2} \left(\frac{2}{u^2 + n/\beta_0}\right)^{\frac{1}{2}(n+1)} \underbrace{\int_0^\infty dt t^{\frac{n}{2}-\frac{1}{2}} e^{-t}} \\
 &= \frac{1}{\sqrt{2\pi}\Gamma(n/2)} \left(\frac{n}{2\beta_0}\right)^{n/2} \left(\frac{2}{u^2 + n/\beta_0}\right)^{\frac{1}{2}(n+1)} \Gamma\left(\frac{n}{2} + \frac{1}{2}\right) . \quad (\text{B.1})
 \end{aligned}$$

For deriving the Gamma distribution $\Gamma(\frac{n}{2} + \frac{1}{2})$ the substitution $t := \frac{n\beta}{2\beta_0} + \frac{\beta u^2}{2}$ was made. Introducing the Tsallis parameter $q = 1 + \frac{2}{n+1}$ the marginal distribution takes the following form:

$$p(u_\tau) \propto \left(1 + \beta_0 \cdot u^2 \left(\frac{q-1}{3-q}\right)\right)^{\frac{1}{1-q}} \quad (\text{B.2})$$

The parameter q defines the form of the PDF, similar to λ^2 for the lognormal model. For $q \rightarrow 1$ a Gaussian distribution is obtained, q -values larger than 1 indicate intermittent distributions.

Appendix C

Offset of the Conditional Moments

Numerator and denominator of the integral γ_1 can be calculated separately. The integral then reads:

$$\begin{aligned}\gamma_1(\mathbf{y}, \sigma) &= \frac{\int_{-\infty}^{\infty} dx (x - \mathbf{y}) \cdot \exp\left(-\frac{x^2}{2s^2} - \frac{(x-\mathbf{y})^2}{2\sigma^2}\right)}{\int_{-\infty}^{\infty} dx \exp\left(-\frac{x^2}{2s^2} - \frac{(x-\mathbf{y})^2}{2\sigma^2}\right)} \\ &= \frac{\sqrt{\frac{2\pi}{s^{-2} + \sigma^{-2}}} \cdot \left(-\frac{\sigma^2 \mathbf{y}}{\sigma^2 + s^2}\right) \cdot \exp\left[\frac{s^2 \mathbf{y}^2}{2(\sigma^4 + s^2 \sigma^2)} - \frac{\mathbf{y}^2}{2\sigma^2}\right]}{\sqrt{\frac{2\pi}{s^{-2} + \sigma^{-2}}} \cdot \exp\left[-\frac{\mathbf{y}^2}{2(\sigma^2 + s^2)}\right]} \\ &= -\frac{\sigma^2 \mathbf{y}}{\sigma^2 + s^2} \cdot \exp\left[\frac{\sigma^2 \mathbf{y}^2 + s^2 \mathbf{y}^2 - \mathbf{y}^2(\sigma^2 + s^2)}{2(\sigma^4 + \sigma^2 s^2)}\right] \\ &= -\mathbf{y} \cdot \frac{\sigma^2}{\sigma^2 + s^2} \cdot\end{aligned}\tag{C.1}$$

Analogously γ_2 can be obtained. The denominator is the same as for γ_1 and the numerator Z reads:

$$Z = \sqrt{\frac{2\pi}{s^{-2} + \sigma^{-2}}} \cdot \left(\frac{\sigma^2(s^4 + \sigma^2 s^2 + \sigma^2 \mathbf{y}^2)}{(\sigma^2 + s^2)^2}\right) \cdot \exp\left[\frac{s^2 \mathbf{y}^2}{2(\sigma^4 + s^2 \sigma^2)} - \frac{\mathbf{y}^2}{2\sigma^2}\right] \cdot$$

Therefore the integral γ_2 is found to be:

$$\gamma_2(\mathbf{y}, \sigma) = \frac{\sigma^2(s^4 + \sigma^2 s^2 + \sigma^2 \mathbf{y}^2)}{(\sigma^2 + s^2)^2} \cdot\tag{C.2}$$

Danksagung

Mein Dank geht an all diejenigen, die mich während meiner Promotionsphase unterstützt haben. Vor allem möchte ich Prof. Dr. Joachim Peinke für die sehr gute Betreuung während der Arbeit aber auch abseits von ihr danken.

Ferner möchte ich mich bei den Mitgliedern der Arbeitsgruppe Hydrodynamik für die freundliche und zugleich produktive Arbeitsatmosphäre bedanken, das sind Malte Siefert, Matthias Wächter, Andreas Nawroth, Marco Munzel, Mathias Karth, Michael Hölling, Amjed Mohammed, Thorsten Schneider, Janet Neerken, Thomas Bohlen, Udo Kulschewski und Peter Neumeyer, sowie René Grüneberger und Wilhelm Jürgens. Insbesondere Dr. Stephan Barth möchte ich für die Korrektur der Arbeit und hilfreiche Anregungen danken.

Priv. Doz. Dr. Achim Kittel danke ich für die Zeit, die er sich für die Begutachtung dieser Arbeit nahm.

Ein ganz besonderer Dank abseits der Arbeit geht natürlich an meine Familie, an Jessica und Tristan.

Lebenslauf

Persönliche Daten

Name Frank Böttcher
Geburtsdatum 17.02.1975
Geburtsort Nienburg/Weser
Nationalität deutsch

Schulausbildung

1981 - 1985 Grundschule Landesbergen
1985 - 1987 Orientierungsstufe Stolzenau
1987 - 1994 Gymnasium Stolzenau

Studium

04.1995 - 08.1999 Studium der Wirtschaftswissenschaften an der Carl von Ossietzky Universität Oldenburg (Abschluss: Vordiplom)
10.1995 - 01.2001 Studium der Physik an der Carl von Ossietzky Universität Oldenburg (Abschluss: Diplom)
12.1999 - 12.2000 Diplomarbeit im Fachbereich Physik der Carl von Ossietzky Universität Oldenburg, Arbeitsgruppe Hydrodynamik unter Prof. Dr. J. Peinke, mit dem Titel:
'Untersuchung der kleinskaligen Turbulenz im atmosphärischen Windfeld mit Hilfe statistischer Methoden'

Wissenschaftliche Arbeit

10.2001 - 02.2005 Promotion an der Carl von Ossietzky Universität Oldenburg, Arbeitsgruppe Hydrodynamik unter Prof. Dr. J. Peinke

Erklärung

Ich erkläre hiermit, dass

- (a) eine Promotion zum Dr. rer. nat. angestrebt wird,
- (b) ich diese Arbeit selbstständig verfasst und nur die angegebenen Hilfsmittel benutzt habe, und dass die Arbeit in Teilen bereits veröffentlicht bzw. zur Veröffentlichung eingereicht wurde,
- (c) diese Dissertation weder in ihrer Gesamtheit noch in Teilen einer anderen Hochschule zur Begutachtung in einem Promotionsverfahren vorgelegen hat.

Oldenburg, den 17. Dezember 2004

.....

(Frank Böttcher)

Publikationsliste

der in dieser Arbeit enthaltenen Veröffentlichungen

F. BÖTTCHER, CH. RENNER, H.-P. WALDL AND J. PEINKE. On the statistics of wind gusts. *Bound.-Layer Meteor.*, 108(1-2):163-173, 2003.

'J. Peinke hatte bei dieser Arbeit eine betreuende Funktion. Ch. Renner und H.-P. Waldl gaben Anregungen während der Entstehung des Artikels. Die wissenschaftliche Ausarbeitung stammt von mir.'

F. BÖTTCHER, ST. BARTH AND J. PEINKE. Small and large scale fluctuations in atmospheric wind speeds. eingereicht in *Stoch. Environ. Res. Risk Assess.*

'J. Peinke hatte bei dieser Arbeit eine betreuende Funktion. St. Barth gab Anregungen zum Aufbau des Artikels. Die wissenschaftliche Ausarbeitung stammt von mir.'

F. BÖTTCHER AND J. PEINKE. A generalized method to distinguish between dynamical and measurement noise in complex dynamical systems. *zu veröffentlichen*

'J. Peinke hatte bei dieser Arbeit eine betreuende Funktion. Die wissenschaftliche Ausarbeitung stammt von mir.'

Die Anteile der aufgeführten Autoren entsprechen den Angaben.

Oldenburg, den 17. Dezember 2004

.....
(Prof. Dr. J. Peinke)

Weitere Publikationen mit meiner Beteiligung

- J. PEINKE, ST. BARTH, F. BÖTTCHER, D. HEINEMANN, B. LANGE. Turbulence, a challenging problem for wind energy. *Physica A*, 338:187-193, 2004.
- J. PEINKE, F. BÖTTCHER AND ST. BARTH. Anomalous statistics in turbulence, financial markets and other complex systems. *Ann. Phys.*, 13:450-460, 2004.
- F. BÖTTCHER, CH. RENNER, H.-P. WALDL UND J. PEINKE. Problematik der Windböen. *DEWI Magazin*, 19:58-62, 2001.

Vorträge und Proceedings

- F. BÖTTCHER, M. SIEFERT AND J. PEINKE. A generalized method to distinguish between dynamical and measurement noise in complex dynamical systems. Physics in Signal & Image Processing, Talk and Proceedings, Toulouse, 01/2005
- F. BÖTTCHER AND J. PEINKE. Wind gusts and heavy-tailed statistics in atmospheric velocities. 5. Dresdener Herbstseminar des Arbeitskreises Nichtlineare Physik, Vortrag, MPI Dresden, 11/2004.
- F. BÖTTCHER AND J. PEINKE. Extreme statistics in atmospheric velocity time series. EGU – 1st General Assembly, Vortrag, Nice, 04/2004.
- F. BÖTTCHER, M. SIEFERT, E. ANAHUA AND J. PEINKE. Analysis of noisy and deterministic contributions to the dynamics of measured data sets. EGS – AGU – EUG Joint Assembly, Vortrag, Nice, 04/2003.
- F. BÖTTCHER AND J. PEINKE. Dynamical features of atmospheric wind gusts. 3. Dresdner Herbstseminar des Arbeitskreises Nichtlineare Physik, Hauptvortrag, MPI Dresden, 12/2002.
- F. BÖTTCHER, E. ANAHUA AND J. PEINKE. Dynamische Eigenschaften von Windböen und ihre Auswirkungen. Proceedings, DEWEK, Wilhelmshaven, 11/2002.
- F. BÖTTCHER, E. ANAHUA AND J. PEINKE. The dynamical behavior of gusts. Proceedings, Global Wind Power, Paris, 04/2002.

- F. BÖTTCHER, H.-P. WALDL, UND J. PEINKE. On the statistics of gusts.
European Geophysical Society XXVI General Assembly, Vortrag, Nice,
03/2001.